Thermodynamic and Structural Properties of CuCrO 2 and CuCr 2 O 4 : Experimental Investigation and Phase Equilibria Modeling of the Cu–Cr–O System

J. Schorne-Pinto, P. Chartrand, A. Barnabé, Laurent Cassayre

Thermodynamic and structural properties of $CuCrO_2$ and $CuCr_2O_4$: Experimental investigation and phase equilibria modeling of the Cu-Cr-O system

J. Schorne-Pinto† [1,2] , P. Chartrand [3], A. Barnabé [2], L. Cassayre* [1]

[1] Laboratoire de Génie Chimique, Université de Toulouse, CNRS, INP, UPS, Toulouse, France

[2] CIRIMAT, Université de Toulouse, CNRS, UT3 - Paul Sabatier, 31062 Toulouse cedex 9 - France

[3] Centre for Research in Computational Thermochemistry, Polytechnique Montréal, Montréal, PQ, Canada H3C 3A7.

KEYWORDS. Mixed oxides, Cr-Cu-O system, delafossite $CuCrO_2$, spinel $CuCr_2O_4$, thermodynamic model, Calphad method.

ABSTRACT: This work considers the equilibria between the stable phases of the Cr-Cu-O ternary chemical system, at atmospheric pressure and in a large temperature range that includes the high-temperature liquid phase. Based on a thorough evaluation of literature data, we performed complementary experimental investigations of solid phase properties (especially the mixed oxides), by implementation of spark plasma sintering and microanalysis, high-temperature X-ray diffraction combined with Rietveld analysis, differential thermal analysis and thermogravimetry. We show that neither the spinel $CuCr_2O_4$ nor the delafossite $CuCrO_2$ phases exhibit significant cationic non-stoichiometry. We provide an assessment of the thermodynamic functions of the spinel up to 1200 K, taking into account the α/β phase transition. We propose, for the first time, a consistent thermodynamic description of the Cr-Cu-O system based on the Calphad method, allowing the computation of reactions and phase equilibria, including the high-temperature liquid phase described by the Modified Quasichemical Model.

1 Introduction

This work considers the equilibria between the stable phases of the Cr-Cu-O chemical system, at atmospheric pressure and in a large temperature range that includes the high-temperature liquid phase. Apart from the simple components (pure elements and simple oxides), and according to Perrot's literature review [1] published in 2010, this system contains three stable mixed oxide phases which are of high applicative interest in various area.

First, the cuprous chromite $CuCrO_2$, also named "MacConnelite" in honor of the geologist Richard Bradford McConnell [2] and occasionally noted as $Cu_2Cr_2O_4$ in older works, crystallizes in a rhombohedral structure (delafossite type, space group $R\bar{3}m$, Fig. 1(a)) [3] and it is one of the most encouraging candidates as transparent p-type conducting oxide in optoelectronic devices [4–6]. This phase presents also interest in thermoelectric applications [7–9], catalytic/photocatalytic [10–13], photocathode in dye sensitized solar cells (DSSC) [14–16], water splitting / H_2 production [12,17] and multiferroic behavior [18,19]. Second, the copper chromite $CuCr_2O_4$ presents a tetragonally distorted spinel structure (hausmannite type, space group $I4_1/amd$, Fig. 1(b)) at room temperature, and transforms to cubic structure (spinel type, space group $Fd\bar{3}m$, Fig. 1(c)) through a transition involving the cooperative Jahn–Teller distortion at 580 ± 5 ^{0}C [20,21]. This spinel phase has wide commercial application as catalysts in organic synthesis process [22–24], H_2 production [25], photovoltaic [25,26]. Third, the copper chromate $CuCrO_4$ compound (space group *Cmcm*, Fig. 1(d)) is also stable under pO_2 = 1 atm [27]. This phase contains chromium at oxidation degree +VI, which is toxic and prohibited in some major safety regulations, e.g., European Union regulation REACH (Registration, Evaluation, Authorisation, and Restriction of Chemicals).

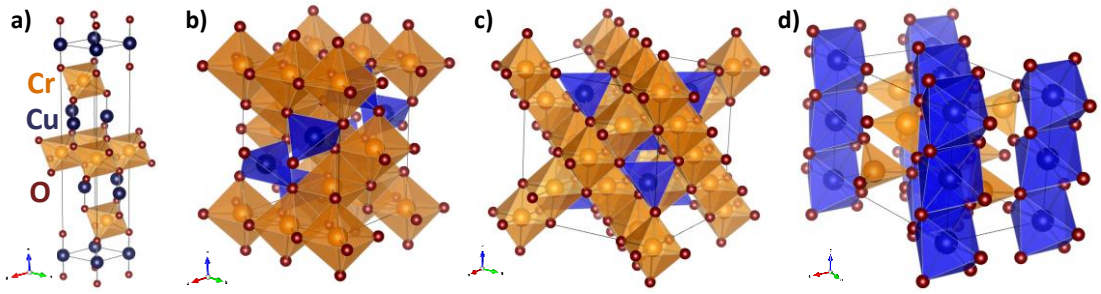

Fig. 1: Crystal structure of (a) $CuCrO_2$ delafossite ($R\bar{3}m$), (b) tetragonal β-$CuCr_2O_4$ spinel ($I4_1/amd$), (c) cubic α-$CuCr_2O_4$ spinel ($Fd\bar{3}m$), and (d) copper chromate $CuCrO_4$ ($Cmcm$).

While thermodynamic modeling has been widely implemented in the last decade to describe thermodynamic properties and phase relationships in ternary or higher order oxide systems (e.g. Al-Mg-O [28], Cu-Fe-O [29], Al-Fe-O [30], and Fe-V-O [31]), there is currently no unified thermodynamic description of the Cu-Cr-O system that would allow phase diagram or chemical reaction computations. With the general objective of describing the phase equilibria in this system, we present an overview of the available literature data [27,32–34] in the next sections.

1.1 Phase equilibria in the Cr-Cu-O system

A compilation of the published temperatures for the invariants of the Cr-Cu-O system, in air (pO_2 = 0.21 atm) and/or pure oxygen (pO_2 = 1 atm), is presented in Table 1. As highlighted in Perrot's review [1], the invariant reactions temperature have been measured by many authors, with large discrepancies between some of them (e.g., formation temperature of $CuCrO_2$ from $CuCr_2O_4$ and CuO).

Table 1: Published temperature (^{0}C) for phase transitions in the Cr-Cu-O system

Phase transition	*Atm*	*Schmahl [35]*	*Gadalla [32]*	*Jacob [33]*	*Other*
$Cr_2O_3(s) \rightarrow Cr_2O_3(l)$	*Air*	-	-	-	*2330 [36]*
$2CuO(s) \rightarrow Cu_2O(s) + 0.5O_2(g)$	*Air*	-	*1026[↓]*	*1028[↓]*	*1031 ± 2 [37]*
$Cu_2O(s) \rightarrow Cu_2O(l)$	*Air*	-	*1162[↓]*	*1149[↓]*	*1125 [38]*
$2CuCrO_4(s) \rightarrow CuCr_2O_4(s) + CuO + 1.5O_2(g)$	*O_2*	-	-	*462 ± 10*	*467 [27]*
	Air	-	-	*426 ± 10*	*425 [27]*
$CuCr_2O_4(s) + CuO(s) \rightarrow 2CuCrO_2(s) + 0.5O_2(g)$	*O_2*	*876*	*938*	*894 ± 10*	*900 [27]*
	Air	*774*	*890*	*792 ± 10*	*800 [27]*
$2CuCr_2O_4(s) \rightarrow 2CuCrO_2(s) + Cr_2O_3(s) + 0.5O_2(g)$	*O_2*	-	*1222*	-	-
	Air	*1009*	*1107*	*1012*	*987 [39]*
$CuCrO_2(s) + Cu_2O(s) \rightarrow Liquid$ (Eutectic)	*O_2*	-	*1100*	-	-
	Air	-	*1130*	*1127*	*1112±2, 0.0194 at.% [34]*
$CuCrO_2(s) \rightarrow CuCrO_2(l)$	*O_2*	-	-	-	-
	Air	-	*> 1560*	-	*1893*[40]

** Obtained by theoretical method; [↓] Extracted from phase diagram.*

Recently, the liquidus region and the coordinates of the eutectic point of the Cu-Cr-O system in air have been revisited by Hamuyuni and Taskinen [34] thanks to careful experimental work. As indicated in Table 1, a temperature of 1112 ± 2 ^{0}C has been established, instead of 1130 ^{0}C proposed by Gadalla and White [32]. The eutectic composition,

measured by the quenching method coupled with chemical analysis using Electron Probe Microanalysis (EPMA) technique, has been proposed as 2.06 wt.% Cr_2O_3 (x = 0.0194 in molar fraction). These data are shown in Fig. 2 together with the experimental phase diagrams proposed by Gadalla and White [32] and Jacob *et al.* [33].

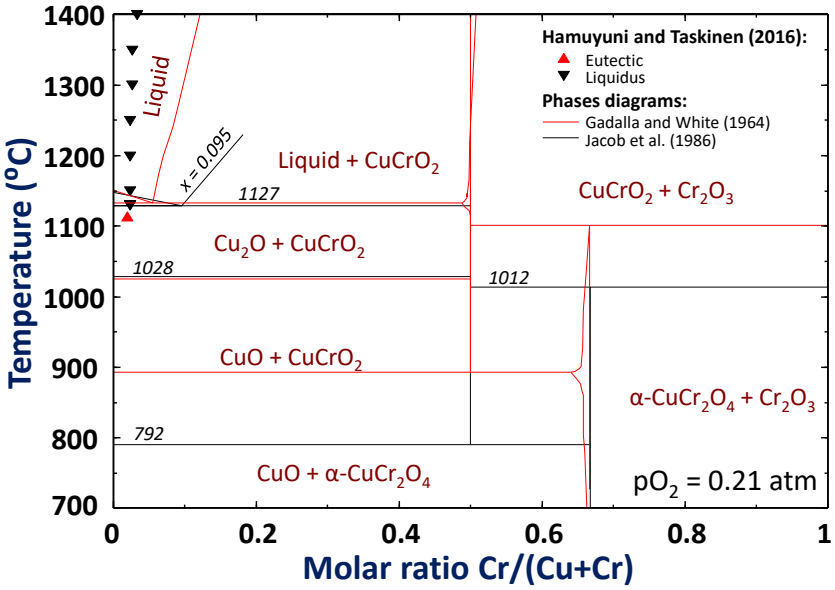

Fig. 2 : Phase diagram of the Cu-Cr-O system in air, according to Gadalla and White[32] (dashed red lines) and Jacob et al. 33 (solid black lines, including their values of transition temperature). These phase diagrams have been replotted from Phase Equilibria Diagrams Database ®. Recent experimental points published by Hamuyuni and Taskinen[34] are indicated with triangles.

One can note from Fig. 2 that the equilibrium between $CuCrO_2$ and $CuCr_2O_4$ strongly differs from a phase diagram to the other. Indeed, Gadalla and White [32] determined the formation temperature for the $CuCrO_2$ phase at 890 °C using thermo-analysis, while, 20 years later, Jacob *et al.* [33] proposed a much lower temperature (792 ± 10) based on electromotive force (emf) measurements. Another remarkable difference is the decomposition temperature of $CuCr_2O_4$, since Jacob *et al.* [33] proposed a temperature of 1012 °C and Gadalla and White [32] 1107 °C. On the other hand, these experimental phase diagrams also present similarities, e.g., CuO ↔ Cu_2O transition and eutectic temperature. However, this eutectic temperature is not in agreement with the recent measurements by Hamuyuni and Taskinen [34].

1.2 Thermodynamic properties and stoichiometry of Cu-Cr-O mixed oxides

The knowledge of thermodynamic properties, such as isobaric heat capacity (c_p), standard enthalpy of formation ($\Delta_f H°_{298.15}$), and standard entropy ($S°_{298.15}$) of the mixed oxides of the Cu-Cr-O system, is fundamental to understand the thermal stability of the phases. A short overview of the state of the art is presented in this section.

$CuCrO_2$ delafossite: many authors performed isobaric heat capacity measurements at low-temperature range [41–43] due to its multiferroic behavior [18,19]. Recently, we proposed an assessment of the thermodynamic properties of this phase [44] based on available emf data [33,45], in-house experimental measurements (differential scanning calorimetry and drop calorimetry) and DFT calculations. The resulting thermodynamic properties are: $\Delta_f H°_{298.15}(CuCrO_2) = -670.8 \pm 1.3$ kJ/mol, $S°_{298.15}(CuCrO_2) = 88.89$ J/mol.K and c_p function in the 300-1200 K range.

Small deviations of the cationic stoichiometry have been evidenced in some compounds of the delafossite family, such as $Cu_{1-y}GaO_2$ ($-0.01 \le y \le 0.02$) [46], $Cu_{1+y}Mn_{1-y}O_2$ ($0 \le y \le 0.20$) [47] and $CuFe_{1-y}O_2$ ($0 \le y \le 0.12$) [37] but according to Jacob et al. [33], $CuCrO_2$ is a compound which does not exhibit cationic non-stoichiometry. However several other authors [34,48,49] reported that this phase could accept a chromium deficit in powders (non-stoichiometry in thin-films and nanometric powders are not considered here because of their metastable condition).

β-$CuCr_2O_4$ and α-$CuCr_2O_4$ spinel: these phases present controversial thermodynamic properties in the literature, mainly for the assessment of $\Delta_f H°_{298.15}$ related to the formation reaction from simple oxides CuO and

Cr_2O_3. As shown in Table 2, the estimated value of $\Delta_f H°$ for α-$CuCr_2O_4$ around 1000 K vary from -51.4 [50] to +76 kJ/mol [32]. This is partly due to the fact that the cubic spinel cannot be quenched and stabilized at room temperature [20,21,51].

Table 2: Published values of enthalpy of formation of β and α-$CuCr_2O_4$ spinel from CuO and Cr_2O_3 (adapted from Jacob *et al.* [33] and completed with recent data)

Reference	*Temperature (K)*	$\Delta_f H°$ *(kJ/mol)*	*Method*
Gadalla and White [32]	*1200*	*76*	*Dissociation pressure*
Schmahl and Minzl [35]	*1000*	*3.8*	*Dissociation pressure*
Tretyakov and Schmalzried [50]	*1000 to 1500*	*-51.4*	*emf*
Jacob et al. [33]	*973 to 1353*	*3.7 ± 2.0*	*emf*
Holla [52]	*1123 to 1273*	*-42.2*	*emf*
**Jain et al. [53]*	*0*	*-24.0*	*DFT*
**Muller and Kleppa [54]*	*1173*	*10.42 ± 1.05*	*High-temperature oxide melt solution calorimetry*
**Lilova et al. [55]*	*298.15*	*-25.19 ± 1.83*	*High-temperature oxide melt solution calorimetry*

** Tetragonal β-$CuCr_2O_4$ spinel*

The enthalpy of the tetragonal transition ($I4_1/amd$) ↔ cubic ($Fd\bar{3}m$) was measured by Inaba *et al.* [56] and Lilova *et al.* [55]; the values are - 6.38 kJ (580 ± 5 °C) and - 3.03 kJ (576 ± 2 °C), respectively. This transition should theoretically be first order, however, Inaba *et al.* [56] could not prove it experimentally. Heat capacity measurements have been performed by Inaba *et al.* [56] (400-960 K), Suchomel *et al.* [57] (2-195 K), and Tomiyasu *et al.* [58] (10-273.15 K). These data can be used to evaluate the standard entropy of the phase. According to the work of Jacob *et al.* [33], $CuCr_2O_4$ may exhibit a slight non-stoichiometry corresponding to a Cr/(Cu+Cr) molar ratio between 0.642 and 0.672 at 1150 K (stoichiometric ratio being 0.667). No other study has confirmed these results so far.

$CuCrO_4$: this phase is the least known of the system. Jacob *et al.* [27] evaluated $\Delta_f H°_{298.15}$ = - 815.9 ± 12 kJ/mol and $S°_{298.15}$ = 120.1 ± 14 J/mol.K from emf measurements. According to our knowledge, this is the only thermodynamic assessment available in the literature. The heat capacity was measured by Law *et al.* [59] for temperatures between 0.5 and 20 K, and c_p values beyond this range remain unknown. There is no indication of cationic non-stoichiometry for this phase.

1.3 Objectives of the work

Our review of the literature reveals that the thermodynamic properties and the phase equilibria in the Cr-Cu-O system are not firmly established, and that no thermodynamic model has been proposed so far. Thus, in this work, we have re-investigated the system with new experimental measurements on solid phases, using *in situ* high-temperature X-ray diffraction, thermal analysis and compositional analysis. We paid special attention to the investigation of the cationic stoichiometry of $CuCrO_2$ delafossite and $CuCr_2O_4$ spinel, with the help of a method that we recently implemented on the $CuFeO_2$ delafossite [37]. Then, we propose a thermodynamic model based on the assessment of all available information according to the Calphad method [60].

2 Materials and methods

2.1 Materials

Oxide powder precursors: CuO (ACROS Organics, >99%), Cr_2O_3 (Alfa Aesar, 99.5%) and Cu_2O (Alfa Aesar, 99%) have been used for X-ray diffraction investigations. All samples were prepared by weighing the starting binary oxides in the desired proportions and mixing them in an agate mortar until a homogeneous mixture was obtained. In the rest of the article, compositions are noted using the molar ratio x = Cr/(Cu+Cr) deduced from the weighing.

Delafossite $CuCrO_2$ powder: a polycrystalline sample of $CuCrO_2$ was prepared by a standard solid-state reaction according to a process described in a previous work [61], where Cu_2O and Cr_2O_3 precursors were mixed in stoichiometric quantities in a mortar and then treated at 900 and 1000 °C for 30 h, with intermediate grindings.

Diffusion couple: A Spark Plasma Sintering (SPS) (Fuji 632 Lx) device was used to prepare a bilayer sample where the layers are composed of CuO and Cr_2O_3. The conditions were: pressure of 50 MPa with air atmosphere, tungsten carbide molds, heating rate of 100 °C/min, dwell time of 7 minutes at 750 °C and cooling a rate of 150 °C/min. After obtaining a bilayer sample, the bulk was cut and annealed in a muffle furnace (Nabertherm) under air atmosphere at 975 °C during 120 hours (heating rate of 5 °C/min, cooling rate of 10 °C/min).

2.2 Characterization methods

Composition analysis: the cationic molar ratio of the mixed oxides molar ratio (x = Cr/(Cu+Cr)) was checked by Field Emission Gun Electron Probe Microanalysis FEG-EPMA (SX Five FE, CAMECA) after *in situ* High-Temperature X-Ray Diffraction (HT-XRD) analysis for some samples elaborated from single oxide precursors, and for those obtained from $CuCrO_2$ pristine phase (noted with the letter D). The data are compiled in Table 3.

Table 3 : Samples compositions used in this work, x determined by weighing, and at% measured by microprobe after heat treatment

Reference	*at.%*			
	CuO	*Cr_2O_3*	*$CuCrO_2$*	*Cu_2O*
x = 0.00	*100.00*	-	-	-
x = 0.10	*94.75*	*5.25*	-	-
x = 0.40	*75.00*	*25.00*	-	-
x = 0.44D	-	-	*88.00*	*12.00*
x = 0.50D	-	-	*100.00*	-
x = 0.50	*66.67*	*33.33*	-	-
x = 0.61	*56.11*	*43.89*	-	-
x = 0.80	*33.33*	*66.67*	-	-
x = 1.00	-	*100.00*	-	-

Thermal Analysis: Thermogravimetric Analysis (TGA) was carried out using a Seteram TGA/ DTA 92 instrument in flowing air, in order to measure the formation temperature of the $CuCrO_2$ phase using CuO and Cr_2O_3 as precursors. Samples of around 20 mg were placed in alumina crucibles and heated from 25 to 1100 °C, at heating rate of 5 °C/ min.

Structural analysis: the global structural analysis was performed using *in situ* HT-XRD technique under air. The device was a Bruker D8 diffractometer (λ_{Cu} $K\alpha_1$ = 1.54056 Å and $K\alpha_2$ = 1.54443 Å radiation, nickel filter) equipped with an Anton Parr HTK1200N high-temperature chamber. The HT-XRD patterns were collected from 50 to 1100 °C, under isothermal conditions in steps of 50 °C. The acquisition conditions were 2θ within 15 to 75 °, with a step size of 0.02 ° and counting time of 1.11 s. Crucibles in alumina were used. Phase identification was performed with the DiffracPlus EVA software combined with the PDF database and subsequently refined by Rietveld method using the Full Prof-Win Plot program [62,63].

2.3 Thermodynamic model

The thermodynamic description of the Cr-Cu-O system was established according to the Calphad approach [60], which requires the Gibbs energy function of each of the stable phase in the system. The list of phases and notations used in the present study is given in Table 4. This section details the thermodynamic models implemented for the description of the pure compounds, the metallic phases and the high temperature liquid solution. All calculations were performed with the 7.2 version of the FactSage® software [64].

Table 4: Phases in the Cr-Cu-O system

Phase name	*Model*	*Short notation*
Oxide phases		
Cuprite	*Stoichiometric compound*	*Cu_2O*
Tenorite	*Stoichiometric compound*	*CuO*
Eskolaïte	*Stoichiometric compound*	*Cr_2O_3*

Cuprous chromite	*Evaluated in this work*	$CuCrO_2$
Tetragonal - Cupric chromite	*Evaluated in this work*	β-$CuCr_2O_4$
Cubic - Cupric chromite	*Evaluated in this work*	α-$CuCr_2O_4$
Copper chromate	*Stoichiometric compound*	$CuCrO_4$
Metallic phases		
fcc	*Bragg Williams mixing model : (Cu, Cr, O)*	*fcc*
bcc	*Bragg Williams mixing model : (Cu, Cr, O)*	*bcc*
Liquid (metal and oxide)		
Liquid	*Modified Quasichemical Model : (Cu^{1+}, Cu^{2+}, Cr^{1+}, Cr^{2+}, Cr^{3+})(O^{2-}, Va^{1-})*	*Liquid*

Pure compounds: The Gibbs energy function of a pure compound *i* is given by Eq. 1.

$$G_i^\circ(T) = \Delta H_{298.15}^\circ(i) + \int_{298.15}^{T_0} c_{p_i}^\circ(T)dT - T_0\left(S_{298.15}^\circ(i) + \int_{298.15}^{T_0} \frac{c_{p_i}^\circ(T)}{T}dT\right) \quad \text{Eq. 1}$$

where $\Delta H_{298.15}^\circ(i)$ is the standard enthalpy of formation, $S_{298.15}^\circ(i)$ is the standard entropy, and $c_{p_i}^\circ(T)$ is the isobaric heat capacity expressed by a Maier-Kelly polynomial [65]:

$$c_{p_i}^\circ(T) = \mathrm{a} + \mathrm{bT} + \mathrm{c}T^2 + dT^{-2} + eT^{-0.5} \quad \text{Eq. 2}$$

Metallic phases: The molar Gibbs energies of the fcc and bcc solid phases are described using the Bragg-Williams random mixing model in the form of Redlich-Kister polynomial [66]. The interaction parameters between the metallic end-members Cu and Cr are taken from Cui and Jung [67], and the Cu-O interactions are accepted from Shishin and Decterov [68]. The Cr-O interactions have been reoptimized.

Liquid solution: As summarized in Table 5, several models have been implemented to describe the liquid phase in the binary subsystems of the Cr-Cu-O system, and no unified model has been proposed so far for the ternary system.

Table 5. Overview of the models implemented for the thermodynamic description of the liquid phase of the binary subsystems of the Cr-Cu-O system

Subsystem	*Reference*	*Model name*	*Model representation*
Cu-Cr	*Saunders (1987)* [69]	*Subregular solution model*	*(Cu,Cr)*
	Hämäläinen et al. (1990) [70]	*Subregular solution model*	*(Cu,Cr)*
	Zeng and Hämäläinen (1995) [71]	*Subregular solution model*	*(Cu,Cr)*
	Turchanin (2006) [72]	*Subregular solution model*	*(Cu,Cr)*
	Cui and Jung (2017) [67]	*Modified Quasichemical Model*	*(Cu,Cr)*
Cu-O	*Hallstedt et al. (1994)* [73]	*Ionic liquid model*	$(Cu^{+},Cu^{+2})_P(O^{-2},Va^{-Q})_Q$
	Hallstedt and Gauckler (2003) [74]	*Ionic liquid model*	$(Cu^{+},Cu^{+2})_P(O^{-2},Va^{-Q})_Q$
	Clavaguera-Mora et al. (2004) [75]	*Associate model*	(Cu_2,O,Cu_2O)
	Schramm et al. (2005) [76]	*Ionic liquid model*	$(Cu^{+},Cu^{+2}, Cu^{+3})_P(O^{-2},Va^{-Q})_Q$
	Shishin and Decterov (2012) [68]	*Modified Quasichemical Model*	(Cu^{I},Cu^{II},O)
Cr-O	*Taylor and Dinsdale (1990)* [77]	*Ionic liquid model*	$(Cr^{+3})(O^{-2},Va)$
	Kowalski and Spencer (1995) [78]	*Associate model*	$(Cr,CrO_{1.5})$
	Luoma (2002) [79]	*Associate model*	$(Cr,Cr_{2/3}O)$
	Povoden et al. (2006) [80]	*Ionic liquid model*	$(Cr^{+2},Cr^{+3})_P(O^{-2},Va^{-Q})_Q$

In the present work, the Modified Quasichemical Model (MQM) in the Quadruplet Approximation [82,83] was selected to describe jointly the liquid metal and the liquid slag. The description contains two sublattices: the cationic sublattice is occupied by Cu and Cr cations (i.e., Cu^{1+}, Cu^{2+}, Cr^{1+}, Cr^{2+}, and Cr^{3+}) while the anionic sublattice is occupied by oxygen O^{2-} and vacancies Va^{1-}. The resulting liquid solution is composed of ten end-members: Cu_2O, CuO, CuVa, $CuVa_2$, Cr_2O, CrO, Cr_2O_3, CrVa, $CrVa_2$, and $CrVa_3$, where Va represents an electron temporarily localized on an anionic site. In that way, the CuVa end-member represents liquid metallic copper, with the same thermodynamic functions as Cu(liq). Likewise, CrVa represents liquid metallic chromium, with functions equal to Cr(liq). $CuVa_2$, $CrVa_2$, and $CrVa_3$ have no physical meaning and they are thus highly destabilized relative to CuVa, and CrVa end-members in the model.

For the description of the $(Cu,Cr)O_x$ liquid solution, the quasichemical reaction is defined as:

$$(Cu-O-Cu)+(Cr-O-Cr)=2(Cu-O-Cr)\quad \Delta g_{CuCr/O} \qquad \text{Eq. 3}$$

where $\Delta g_{CuCr/O}$ is a composition independent parameter, whose value is determined from the optimization of the Cr-Cu-O liquid solution.

In this system, the composition of maximum Short-Range Ordering (SRO) comes from the selection of cation-cation Second-Nearest-Neighbour (SNN) coordination numbers $Z^{Cu}_{CuCr/OO}$ and $Z^{Cr}_{CuCr/OO}$. Additional improvement in the quadruplet approximation [84] was made using the parameter ζ, which represents the ratio between the 2nd and 1st nearest neighbor coordination numbers. A full description of MQM application to describe liquid phases can be found elsewhere [82].

3 Experimental results

3.1 Formation temperature of the solid phases in air

The solid-state reactions between CuO (tenorite, monoclinic structure, space group C2/c) and Cr_2O_3 (eskolaïte, trigonal structure, space group $R\bar{3}c$) were evaluated via in situ HT-XRD and Rietveld refinement. The XRD patterns for the samples x = 0.10, 0.40, 0.50 and 0.61 over the 50-1100 °C temperature range are presented in Fig. 3, for both heating (Fig. 3(a)) and cooling (Fig 3(b)). The XRD patterns for pure eskolaïte (x = 1.00) are not shown here because this phase is stable over the entire temperature range. The HT-XRD patterns of the pure copper oxide (x = 0.00) (not shown here either because already shown in our previous work on the Cu-Fe-O system [37]) indicate that the complete reduction of tenorite CuO into cuprite Cu_2O described by the Eq. 4 occurs between 1000 and 1050 °C, which is consistent with literature data (Table 1).

$$2\,CuO(s)\ \rightarrow Cu_2O(s)+\ 0.5\,O_2(g) \qquad \text{Eq. 4}$$

For the intermediate compositions, the pristine oxide CuO and Cr_2O_3 are the only phases detectable during heating up to 700 °C. They start to react at a temperature superior to 750 °C, forming a mixed oxide with spinel structure according to Eq. 5. Although this spinel phase is known to be stable at lower temperature, this result shows that is necessary to reach 700-750 °C to thermally activate the reaction between CuO and Cr_2O_3 and form $CuCr_2O_4$ [8,19]. At this temperature, the spinel phase exhibits a cubic symmetry.

$$Cr_2O_3(s)\ +CuO(s)\rightarrow CuCr_2O_4(s) \qquad \text{Eq. 5}$$

The $CuCrO_2$ delafossite phase then forms in between 750 and 800 °C, for the five mixtures. As CuO, Cr_2O_3 and $CuCr_2O_4$ phases exist in this temperature range, the delafossite phase could be formed either by reaction of the spinel phase with CuO expressed by Eq. 6, or also by its decomposition following Eq. 7:

$$CuCr_2O_4(s)\ +CuO(s)\rightarrow 2\,CuCrO_2(s)+O_2(g) \qquad \text{Eq. 6}$$

$$2\,CuCr_2O_4(s)\ \rightarrow 2\,CuCrO_2(s)+\ Cr_2O_3(s)+0.5\,O_2(g) \qquad \text{Eq. 7}$$

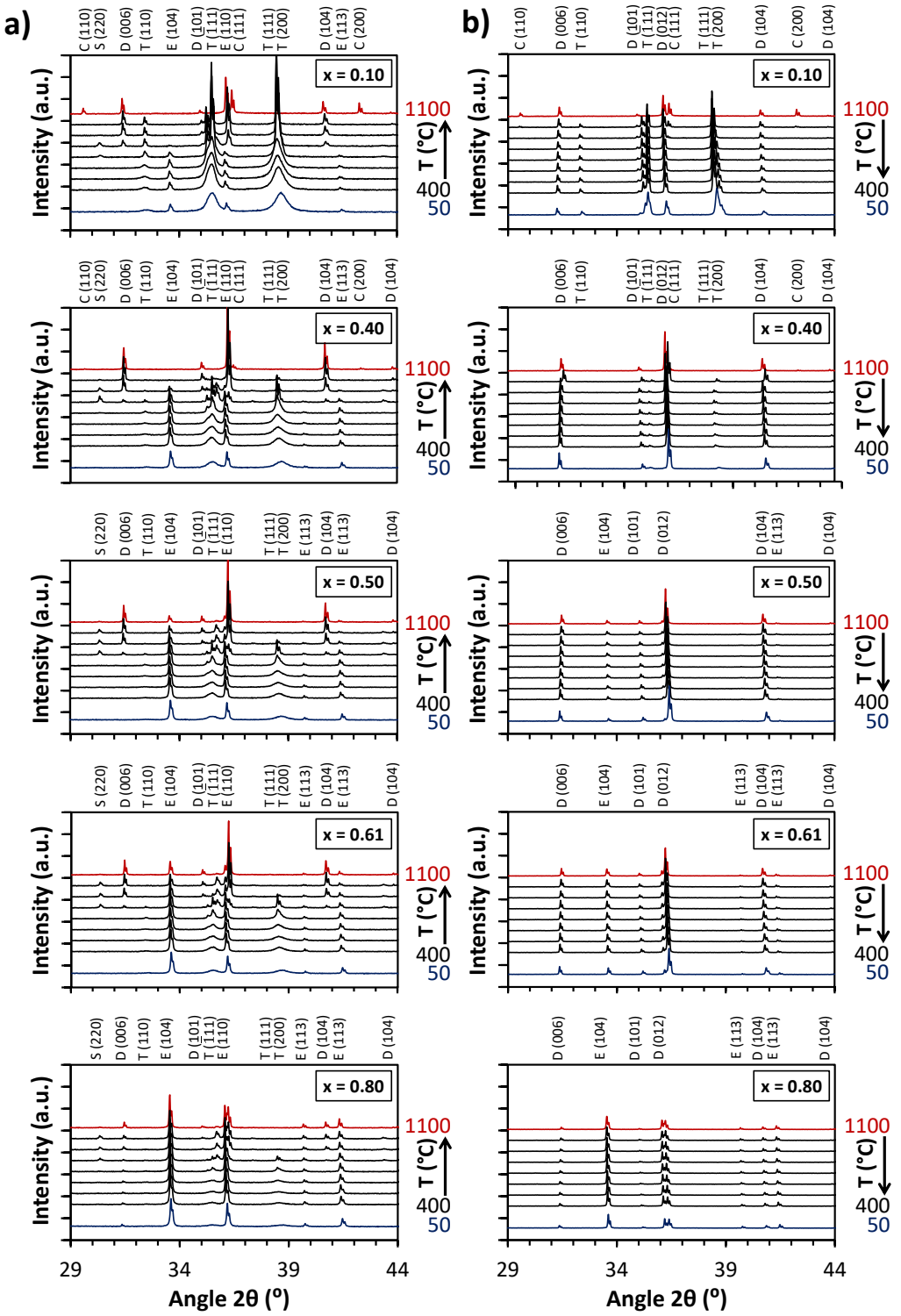

Fig. 3 : (a) XRD patterns for the samples x = 0.10, 0.40, 0.50, 0.61 and 0.80 over the temperature range 50-1100 °C in heating. (b) XRD patterns for the same samples under cooling (E: Eskolaite; T: Tenorite; C: Cuprite; D: Delafossite; and S: Cubic spinel).

The formation of $CuCrO_2$ by direct reaction in between Cr_2O_3 and Cu_2O (Eq. 8) is not considered in this temperature range of 750 – 800°C. Indeed, in our experiments, no Cu_2O is available whatever the composition since

the copper precursor is CuO and the reduction of Cu^{2+} in Cu^{1+} according to Eq. 4 only appears at 1026-1031 °C under p_{O_2} = 0.21 atm (Table 1).

$$Cr_2O_3(s) + Cu_2O(s) \rightarrow 2\ CuCrO_2(s) \qquad \text{Eq. 8}$$

It should be noted that once formed, the delafossite phase does not decompose on cooling (Fig. 3(b)), and therefore these reactions (Eq. 8, Eq. 6 and Eq. 7) are not reversible in air under the HT-XRD timeline, thermodynamically meaning a metastability of this phase over the spinel region.

The thermal behavior of CuO and Cr_2O_3 precursors measured by TGA-DTA in air is presented in Fig. 4. A mass loss (corresponding to the first deviation of the TGA signal) starts at 780 ± 10 °C. It is attributed to the beginning of the formation of the $CuCrO_2$ phase according to (Eq. 6), which releases O_2(g) [33,35]. The oxygen release is caused by the reduction of Cu^{2+} into Cu^{1+} when the spinel phase is transformed into delafossite. An additional event occurs at 1045 °C, corresponding to the reduction of the remaining CuO into Cu_2O which is immediately transformed into delafossite according to Eq. 8, because Cu_2O is not observed in the XRD pattern at 1100°C except for the Cu-rich phases (x = 0.10 and x = 0.40 - minor, Fig. 3).

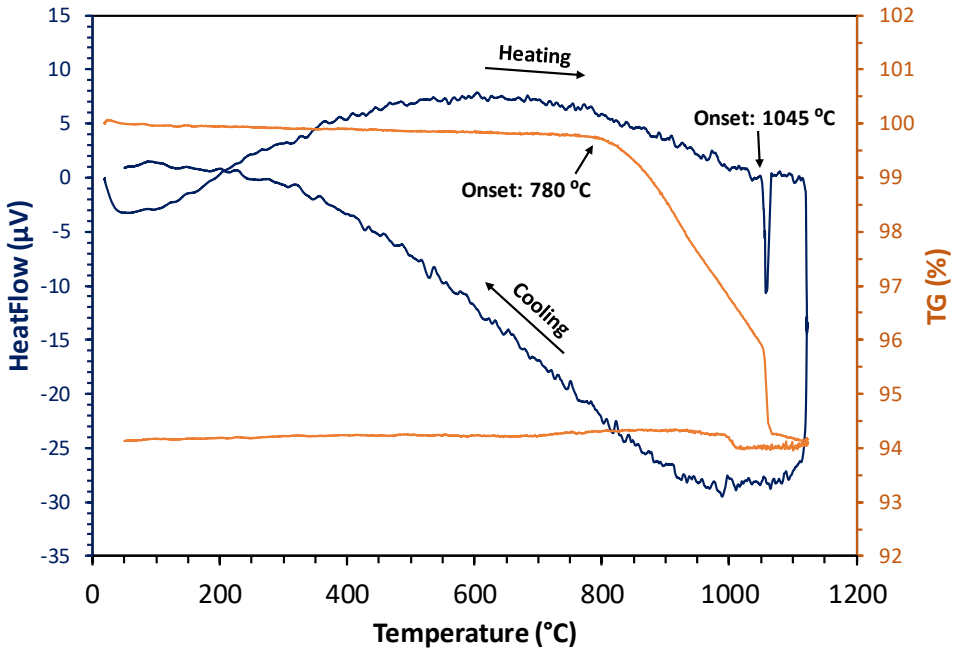

Fig. 4 : TGA-DTA of CuO and Cr_2O_3 precursors (x = 0.50) in air (heating rate 5 °C/min)

A thorough Rietveld analysis was performed for each of the 90 XRD patterns recorded in this work, which gave access to the lattice parameters of each solid phase depending on the system composition and the temperature. As a result, volumetric expansion coefficients for each phase can be estimated.

The analyses showed that, from 800°C, the cubic spinel phase lattice parameters are almost constant whatever the initial composition (a = 8.3781(6), 8.3777(7), 8.3775(6) and 8.3773(8) Å for x = 0.40, 0.50, 0.61 and 0.80 respectively). The $CuCr_2O_4$ volumetric expansion coefficients α_V calculated between 800 and 1000°C are also equivalent for each composition ($\alpha_V^{800°C}$ = 30(2) 10^{-6} K^{-1} in average). Similarly, the delafossite unit cells parameters are almost equal at high temperature whatever the composition (a = 3.0025(2) and c = 17.173(3) Å in average at 800°C, 3.0123(3) and c = 17.196(1) Å in average at 1100°C). After cooling to 50°C, the lattice parameters are still independent of the initial system composition, with a = 2.9802(2) and c = 17.128(1) Å for x = 0.40; a = 2.9804(2) and c = 17.129(1) Å for x = 0.50; a = 2.9804(2) and c = 17.130(1) Å for x = 0.61; a = 2.9803(2) and c = 17.131(1) Å for x = 0.80. The $CuCrO_2$ volumetric expansion coefficients α_V at 50°C calculated in the 50 to 1100°C temperature range, are also equivalent for all the compositions ($\alpha_V^{50°C}$ = 7.5(1) 10^{-6} K^{-1} in average).

Therefore, for both mixed oxide phase $CuCr_2O_4$ and $CuCrO_2$, and within the limits of the technique, a non-stoichiometry associated with a change of the lattice parameters cannot be retained. This also suggests that the cationic distribution is not affected by the composition. This is notably different from the Cu-Fe-O system, for

which we have shown previously that the lattice constants of the spinel phase $Cu_xFe_{3-x}O_4$ depend on the composition [85,86], which is a strong indicator of a non-stoichiometry of the phase.

HT-XRD and Rietveld analysis coupled with TGA-DTA in air in the 50 to 1100°C temperature range allow to confirm the existence of the mixed phases described by the literature in this system. The delafossite formation temperature was measured in between 750 and 800°C by HT-XRD and at 780 ± 5°C by TGA, in good agreement with the temperature (792 ± 10) proposed by Jacob *et al.* [33]. The measurement of the structural parameters over the whole range of temperature does not suggest the opening of a non-stoichiometry domain as for the spinel structure in the Fe-like system. As the variations of crystalline parameters can be linked to other phenomena, and since these variations are negligible for some non-stoichiometric delafossite phases, additional measurements were carried out.

3.2 Investigation on the deviation from the stoichiometry of the spinel and delafossite phases

In order to further investigate an eventual cationic non-stoichiometry of the $CuCrO_2$ phase, we performed XRD analysis on a previously synthesized sample composed of pure delafossite phase (x = 0.50D). A known amount of Cu_2O was then added in this sample, leading to the composition x = 0.44D, i.e. $CuCrO_2$ + 12 mol% Cu_2O.

Fig. 5(a) shows the X-ray diffractograms obtained at 50 °C after thermal cycles at a maximum temperature of 1050 °C in air. The structural parameters resulting from the Rietveld refinements are provided in Fig. 5(b).

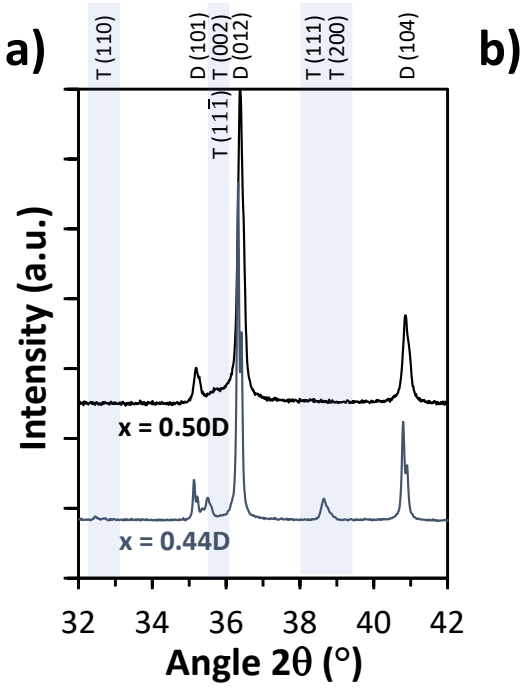

b)

Lattice parameters for delafossite

Composition	x = 0.44D	x = 0.50D
Parameter Cell (Å)		
a	2.9757(2)	2.9759(3)
b	17.101(1)	17.104(2)
Z(O)	0.1141(8)	0.1168(14)
Lattice Volume (Å³)		
V	131.14(2)	131.18(3)
Angle (°)		
Cr-O-Cu	117.6(4)	116.4(8)
Bond length (Å)		
Cr-O	1.939(6)	1.918(10)
Cu-O	1.951(14)	1.998(24)
$O\text{-}O_i$	2.976	2.976
$O\text{-}O_{iv}$	2.487	2.421
$O\text{-}O_i$ /$O\text{-}O_{iv}$	**1.197**	**1.229**
Facteurs		
Bragg R-factor	6.52	8.28
Rf-factor	4.56	4.57

Fig. 5 : (a) focus on 32°<2θ<42° of the XRD patterns of pure $CuCrO_2$ (x=0.50D) and $CuCrO_2$ + 12%mol Cu_2O (x=0.44D) powders at 50 °C after thermal treatment at 1050 °C. Indexation of the main Bragg's reflexion of Tenorite (T) and Delafossite (D) are indicated, and the non-overlaid pics of Tenorite highlighted. (b) Delafossite unit cell parameters obtained from Rietveld analysis

For the composition x = 0.50D, only the peaks corresponding to the delafossite phase are detected. For the composition x = 0.44D, additional peaks characteristic of the tenorite phase (CuO) are visible. Thus, the excess copper initially supplied in the form of Cu_2O was not integrated into the delafossite structure but remained in the form of a secondary CuO phase. The Rietveld method allowed to quantify the amount of CuO as 26(3) % mol in the sample, resulting in a global composition of x = 0.43(1), in excellent agreement with the powder composition. Again, the *a* and *c* lattice parameters of $CuCrO_2$ were found constants within the limits of the method uncertainty. As detailed in Fig. 5(b), the delafossite contained in sample x = 0.50D has a volume of 131.18 (3) Å³, while the cell volume is 131.14 (2) Å³ with the addition of Cu_2O (difference of only 0.03%). The samples show virtually identical interatomic distances and angles. The only slight difference appears in the Cu-O bond length and in the distortion

of the CrO_6 octahedra, i.e. in the evolution of the covalency of the metal to oxygen bond. The degree of flattening of the CrO_6 octahedron on the axis of order 3 evaluated by the ratio $d(O\text{-}O)_i$ / $d(O\text{-}O)_{iv}$ [87] indicates that from x = 0.44D to x = 0.50D, this ratio increases from 1.197 to 1.229, i.e. that the covalency of the Cr-O bond tends to slightly increase. At the same time, the d(Cu-O) is slightly increasing from 1.951 to 1.998 Å. This could be correlated to a tiny variation of the overall charge of the cations due to vacancies and/or substitution leading to a change of the repulsion in between cations. This could also be correlated with the width of the Delafossite diffraction peaks which are sharper for x = 0.50D than for x = 0.44D.

We further investigated the delafossite phase not only at the structural level but also in its elemental composition by EPMA analyses. A planar section of the sample x = 0.44D after HT-XRD cycle was prepared. The accumulation conditions have been optimized to minimize the experimental uncertainties, and the total mass fraction of each analysis for Cu, Cr and O elements (21 spots) was above 90% indicating that no extra element was present. The average value obtained for x is 0.497 ± 0.010 with a minimum of 0.492 ± 0.010 and a maximum of 0.500 ± 0.010. Thus, within the accuracy limit of this technique, none of the 21 analyses proves that the $CuCrO_2$ phase can accept an excess of copper (or a deficit of chromium). This corroborates the XRD results. This observation is also in good agreement with the values published by Hamuyuni and Taskinen [34] for the phase analyzed after quenching from higher temperatures (1130, 1200, 1250, 1300, 1350 and 1400 °C), where the minimum Cr content was 0.486 ± 0.010.

Similar to the methodology implemented for the $CuFeO_2$ delafossite phase [37], we completed this investigation by the elaboration and characterization of a diffusion couple (see section 2.1). As shown on SEM micrographs of the cross section of the diffusion couple presented in Fig. 6, the $CuO\text{-}Cr_2O_3$ couple exhibits crystals with very anisotropic morphology in the so-called *mixed zone*, making the preparation and EPMA analyses much more difficult to analyze than the $CuO\text{-}Fe_2O_3$ couple. Several heat treatments, preparation methods and measurement conditions were tested to ultimately obtain a sample with a few areas that could be analyzed. The annealing conditions (975 °C for 120 hours in air in a muffle furnace) was selected because it led to the simultaneous presence of the delafossite and spinel phases, maximizing the diffusion of the elements while avoiding the entire decomposition of $CuCr_2O_4$ into $CuCrO_2$ (Eq. 6). The delafossite $CuCrO_2$ phase systematically presents a rather particular morphology in the form of very anisotropic hexagonal platelets (surface of 20 × 120 µm but thickness limited to less than 1 µm) as illustrated in Fig. 6(b) and (c).

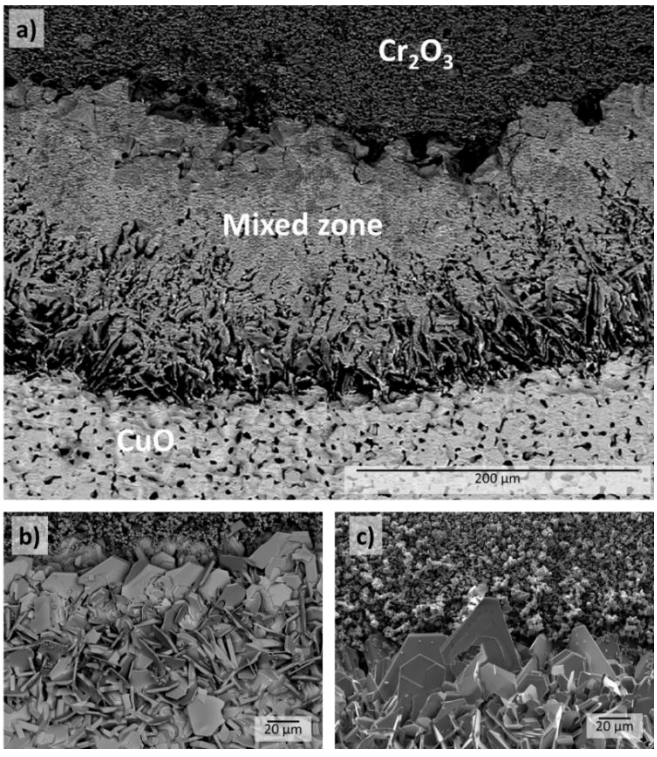

Fig. 6 : SEM-BSE micrographs of the cross section of the diffusion couple prepared by heat treatment of CuO and Cr_2O_3 pellets at 975 °C for 120 h (a) general overview (b) and (c) focus on delafossite platelets

EPMA analysis of the different zones of the diffusion couple provide a detailed picture of the phase compositions (CuO, Cr_2O_3, spinel and delafossite) in the sample. As shown in Table 6, the solubility of Cu in Cr_2O_3 eskolaïte as well as the solubility of Cr in CuO tenorite is very limited. Spinel cationic composition is very stable, with an average of x = 0.67(1), which is corresponds the stoichiometric ratio (0.667). For the delafossite, the average composition of x = 0.51(1) is coherent with a perfectly stoichiometric phase within the accuracy limit. The slight excess of Cr could be correlated to metastable Cu-vacancies as demonstrated in thin films materials by P. L. Popa *et al.* [88]. This is consistent with the width of the diffraction peak as well as the flattening of the CrO_5 octahedra previously observed by XRD experiments. Unlike our previous study that showed the incorporation of copper excess in the $CuFeO_2$ delafossite [37], the present results lead us to conclude that there is no cationic non-stoichiometry in the $CuCrO_2$ delafossite nor in the $CuCr_2O_4$ spinel.

Table 6 : Average of the elemental compositions determined by EPMA in different zones of the diffusion couple

Phase	*N° of points*	*Cu (at%)*	*Cr (at%)*	*O (at %)*	*x*
Spinel	*7*	*14.47(85)*	*29.65(117)*	*55.88(369)*	*0.67(1)*
Delafossite	*10*	*24.52(138)*	*25.88(125)*	*49.60(407)*	*0.51(1)*
Tenorite	*1*	*46.35(61)*	*0.16(3)*	*53.49(141)*	*0.00*
Eskolaïte	*1*	*0.77(8)*	*42.65(60)*	*56.57(137)*	*0.98(1)*

4 Thermodynamic assessment

Based on our selection of literature data and on our new measurements, we provide in this section a full thermodynamic description of the Cr-Cu-O system. The adjusted parameters of this model are related to the properties of the mixed oxide phases as well as the liquid phase. Following the Calphad methodology, the model was built on the assessment of binary sub-systems and then of the ternary system.

4.1 Compounds

The Gibbs energy functions for all compounds considered in our model are listed in Table 7. Simple oxides were taken from existing databases, while mixed oxides ($CuCrO_2$ and $CuCr_2O_4$) were re-evaluated from experimental data available in the literature, as discussed in section 4.3.

Table 7 : Thermodynamic functions of solid and liquid pure phases considered in this work. Units in J/mol or J/mol.K

Phase	*T(K)*	*$\Delta H°_{298.15}$*	*$S°_{298.15}$*	*$c_P°(T)$*	*Ref*
Cu(fcc)	*298.15-1357.77*	*0*	*33.15*	*$24.112 + 5.314.10^{-3}T - 104956T^{-2} - 7.753.10^{-7}T^2$*	*89*
	1357.77-3200			*$31.30 - 3.2775.10^{31}T^{-10}$*	*89*
Cu(l)	*298.15-1357.77*	*12964.744*	*42.6619*	*$24.112 + 5.314.10^{-3}T - 104956T^{-2} - 7.753.10^{-7}T^2 + 2.4565.10^{-19}T^6$*	*89*
	1357.77-3200			*31.38*	*89*
Cr(bcc)	*Magnetic properties: $T_c = -311.50$; $\beta_{mag} = -0.008$*				*89*
	298.15-2180	*9.681*	*23.5698*	*$26.908 - 3.7887.10^{-3}T - 278500T^{-2} + 8.863.10^{-6}T^2$*	*89*
	2180-6000			*$50 + 2.5967T^{-10}$*	*89*
Cr(l)	*298.15-2180*	*24349.633*	*34.9900*	*$26.908 - 3.7887.10^{-3}T - 278500T^{-2} + 8.863.10^{-6}T^2 - 9.9798.10^{-20}T^6$*	*89*
	2180-6000			*50*	*89*
$O_2(g)$	*298.15-1000*	*0*	*205.0330*	*$22.271 + 2.03955.10^{-2}T + 153460T^{-2} - 7.94215.10^{-6}T^2$*	*89*
	1000-3300			*$33.6276 + 2.3832T - 1051620T^{-2} - 8.1372.10^{-8}T^2$*	*89*
	3300-6000			*$37.9072 + 1.70097T - 17532800T^{-2} - 1.28652.10^{-7}T^2$*	*89*

CuO(s)	*298.15-3000*	*-155192.112*	*43.0626*	*49.03 + 6.94.10^{-3}T – 780000T^{-2}*	*90*
CuO(l)	*1673-3000*	*-123946.897*	*44.6560*	*67.56*	*90*
Cu$_2$O(s)	*298.15-3000*	*-170258.185*	*92.6796*	*66.26 + 1.592.10^{-2}T – 748000T^{-2}*	*90*
Cu$_2$O(l)	*298.15-1000*	*-105326.196*	*134.6737*	*65.511 + 1.6488.10^{-2}T -701971.44T^{-2}*	*64*
	1000-2000			*99.914*	*64*
CrO(l)	*298.15-1800*	*-274955.09*	*90.1126*	*56.7277 + 2.7367.10^{-3}T - 1545346.4T^{-2} + 8912.35T^{-1} -507T$^{-0.5}$*	*64*
	1800-2000			*62.76*	*64*
Cr$_2$O(l)	*298.5-1800*	*-250605.457*	*125.3214*	*83.6357 – 1.052.10^{-3}T - 1823846.4T^{-2} + 8.863.10^{-6}T^2 - 9.9798.10^{-20}T^6 + 8912.35T^{-1} -507T$^{-0.5}$*	*64*
	1800-2180			*89.668 – 3.7887.10^{-3}T – 278500T^{-2} + 8.8633.10^{-6}T^2 - 9.980.10^{-20}T^6*	*64*
	2180-6000			*112.76*	*64*
Cr$_2$O$_3$(s)	*Magnetic properties: $T_{Néel}$ = -306 ; β_{mag} = 1.938*				*64*
	298.15-3000	*-1127120*	*84.7710*	*121.44 + 7.8.10^{-3}T – 2000000T^{-2} +3.10-7T^2*	*64*
Cr$_2$O$_3$(l)	*298.15-1800*	*-1009812.182*	*130.8566*	*141.819 + 6.842.10^{-3}T - 3863366.1T^{-2} + 22280.885T^{-1} - 1267.493T$^{-0.5}$*	*64*
	1800-4500			*156.6908*	*64*
CuCrO$_2$(s)	*Magnetic properties: $T_{Néel}$ = 24 ; β_{mag} = 3.89*				*42*
	298.15-1300	*-674200*	*88.6*	*102.564 – 28715954T^{-3} – 128542T$^{-1.5}$*	*44,**
β-CuCr$_2$O$_4$(s)	*Magnetic properties: T_{Curie} = 125; β_{mag}= 1.56*				*58*
	298-800	*-1302002*	*130.46*	*175.169 + 9.88.10^{-3}T - 3857479.7T^{-2}*	***
	800-853			*259482.92 – 440.91T - 26542062809.1T^{-2} + 0.2107723T^2*	***
	853-877			*4602993.98 - 7097.95T - 572669454120.29T^{-2} + 3.07704T^2*	***
	877-1200			*137.143 + 3.08.10^{-2}T*	***
α-CuCr$_2$O$_4$(s)	*298-853*	*-1298972*	*134.0122*	*175.169 + 9.88.10^{-3}T - 3857479.7T^{-2}*	***
	800-853			*259482.92 – 440.91T - 26542062809.1T^{-2} + 0.2107723T^2*	***
	853-877			*4602993.98 - 7097.95T - 572669454120.29T^{-2} + 3.07704T^2*	***
	877-1200			*137.143 + 3.08.10^{-2}T*	***
CuCrO$_4$(s)	*298-1000*	*-821500*	*115.1*	*129.943 + 2.357.10^{-2}T – 1608003.06T^{-2} - 4.9246T^2 -59.3712T$^{-0.5}$*	***

** This work*

4.2 Binary subsystems

The binary subsystems Cu-Cr, Cu-O and Cr-O have been reassessed in order to provide a unified description of the liquid phase with the MQM, and compatibility with the thermodynamic database from the Factsage software [64].

Cu-Cr system: The Cu-Cr subsystem description is taken from Cui and Jung [67]. The fcc phase is described as $(Cu,Cr)_1(Va)_1$, and the bcc phase is described as $(Cu,Cr)_1(Va)_3$. The end-members Gibbs energy functions are reported in Table 7. The liquid phase is described by the MQM as (Cu^{1+},Cu^{2+}, Cr^{1+},Cr^{2+},Cr^{3+})(Va^{1-}), with one interaction term $\Delta g_{Cu^{1+}Cr^{1+}}$. The model parameters are reported in Table 8.

Cu-O system: The thermodynamic functions of the two copper oxides compounds (Cu_2O and CuO) are taken from [90] and provided in Table 7. The liquid phase is described by the MQM as (Cu^{1+}, Cu^{2+})(O^{2-}, Va^{1-}). The $\Delta g_{Cu^{1+}/Va^{1-},O^{2-}}$ and $\Delta g_{Cu^{1+},Cu^{2+}/O^{2-}}$ interaction parameters, whose expression are reported in Table 8, allowed reproducing the numerous available experimental data related to the liquidus temperature in a large composition range [91,92,101,93–100]. The obtained calculated phase diagram (Fig. 7(a)) is in excellent accordance with existing models from Shishin and Decterov [68] (in red in Fig. 7(a)) or Hallstedt and Gauckler [74]. Additionally, Fig. 7(b) shows that the model reproduces well experimental data from [92,97,101,102] in log(pO_2) vs 1/T coordinates.

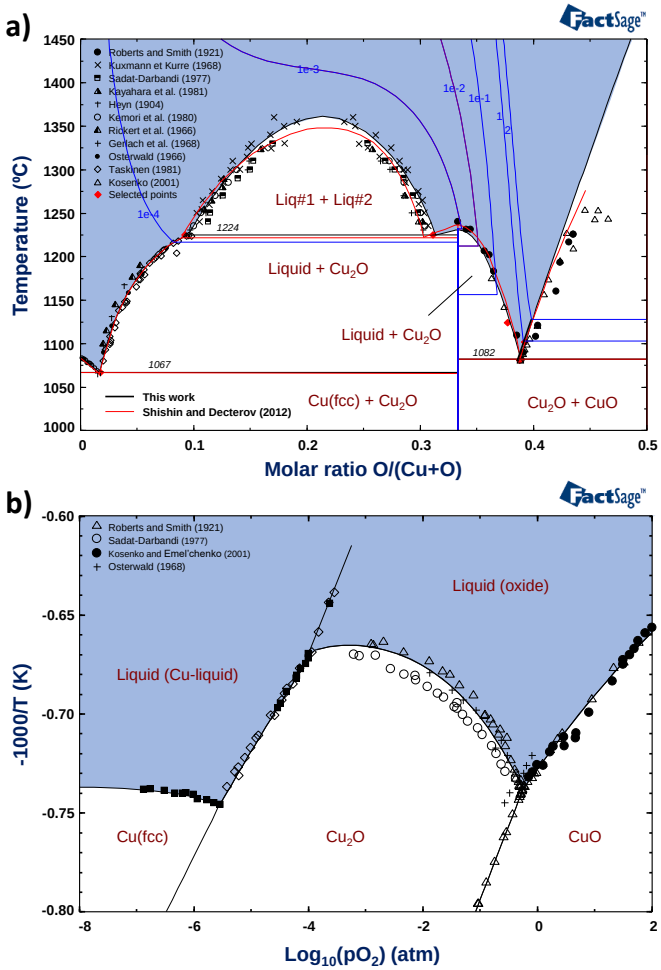

Fig. 7 : (a) Phase diagram of the Cu-O system calculated with our set of parameters, compared to Shishin and Decterov [68] (red lines) and experimental data [91,92,101,93–100]; blue lines represent O_2 isobars; (b) Comparison of pO_2 temperature evolution to experimental data [92,97,101,102].

Cr-O system: The thermodynamic functions of the two chromium oxides compounds (Cr_2O_3 and Cr_3O_4), taken from the FToxid database [64], are provided in Table 7. It has to be noted that the available data related to the oxygen-rich part of this system ($pO_2 \geq 1$ atm; x (O)> 0.667), which contains higher oxidation states of Cr in the phases CrO_3, Cr_5O_{12} and Cr_8O_{21}, were too unreliable to be taken into account. Consequently, the phase diagram does not cover the entire compositional domain. The liquid phase is described by the MQM as $(Cr^{1+}, Cr^{2+}, Cr^{3+})(O^{2-}, Va^{1-})$, and the parameters were adjusted with the experimental data of Toker *et al.* [103] and Ol'shansky and Shlepov [104]. A single interaction ($g^{00}_{Va^-O^{2-}}$) was used to describe the liquid phase (Table 8), mainly because of the lack of experimental data that could help specifying the shape of the miscibility gap between the metal-rich and oxygen-rich liquid phases.

Fig. 8(a) presents the calculated phase diagram, which shows large similarities with the diagram computed by Kjellqvist *et al.* [81] (red lines), as well as older assessments [77–80]. Additionally, Fig. 8(b) shows that the model reproduces well experimental data from Ramsey *et al.* [105] , Davies and Smeltzer [106] and Toker *et al.* [103] in log(pO_2) vs 1/T coordinates.

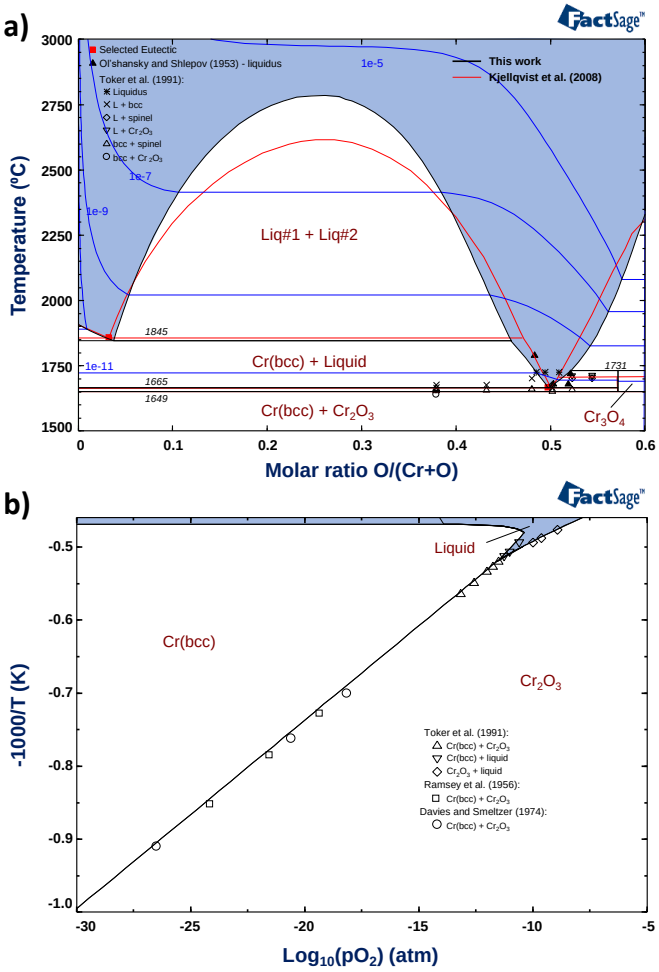

Fig. 8 : (a) Phase diagram of the Cr-O system calculated with our set of parameters, compared to Kjellqvist *et al.* [81] (red lines) and experimental data [103,104]; blue lines represent O_2 isobars; (b) Comparison of PO_2 temperature evolution to experimental data [103,105,106].

4.3 Cr-Cu-O ternary system

Mixed oxides compounds: As concluded from our experimental investigations, the $CuCrO_2$ and $CuCr_2O_4$ oxides do not exhibit significant deviation from stoichiometry. Consequently, we described the Gibbs energy functions of these phases using Eq. 1 (pure compounds). The set of thermodynamic properties resulting from our assessment, discussed in this section, is reported in Table 7.

The heat capacity functions of $CuCr_2O_4$ (β and α) were established in the form of Maier-Kelly polynomial [65] (Eq. 2) using the recent low temperature measurements from Tomiyasu *et al.* [58] (10-273.15 K) and the high-temperature data from Inaba *et al.* [56] (400-960 K). These data are presented in Fig. 9(a) and compared with the Neumann-Kopp estimation [107] based on the simple oxides (CuO and Cr_2O_3). An interpolation was made to estimate the heat capacity up to 298.15 K, and, using Eq. 9, we determined the standard entropy at 298.15 K. The resulting value is $S°_{298.15}(CuCr_2O_4)$ = 130.46 ± 1 J/mol.K, which is in excellent agreement with the value of 130.5 ± 9.2 J/mol.K proposed by Kubaschewski *et al.* [108].

$$S°_{298.15}(CuCr_2O_4) = \int_0^{298.15} \frac{c_p(T)}{T} dT \qquad \text{Eq. 9}$$

The heat capacity functions of $CuCrO_2$ were taken from our previous work [44] (presented in Fig. 9(b) with all available experimental data [41–44,109]), with a small adjustment. The value of $\Delta_f H°_{298.15}(CuCrO_2)$ was adjusted to 674.2 kJ/mol (Table 7), 3.3 kJ/mol greater than previous accepted [44]. The $S°_{298.15}(CuCrO_2)$ was adjusted to 88.6

J/mol.K, 0.29 J/mol.K smaller than our proposed value [44]. These minor changes have been made to ensure the best coherence of high temperature equilibria data with the $CuCr_2O_4$ phase.

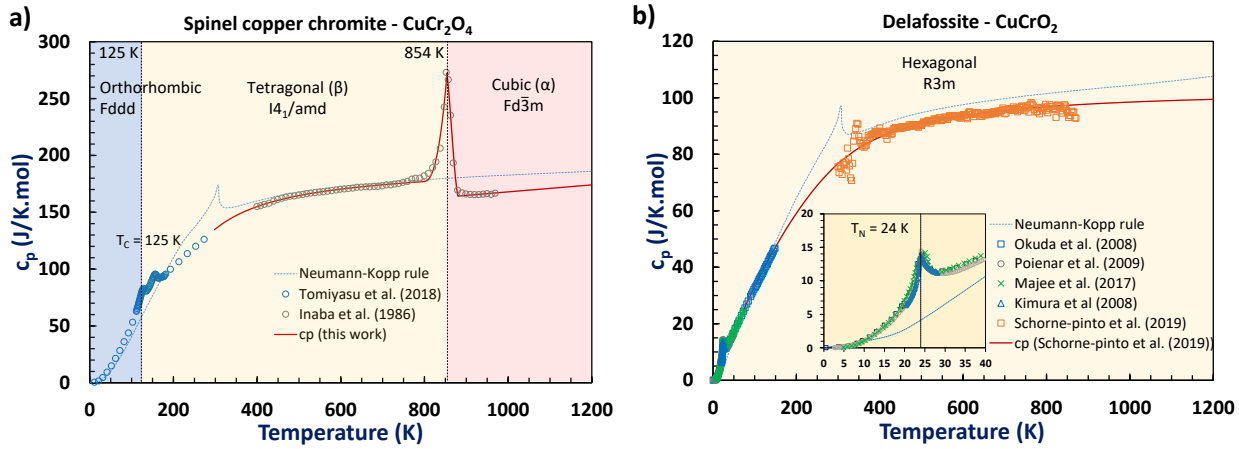

Fig. 9 : (a) Calculated heat capacity of $CuCr_2O_4$ and literature data [56,58]. (b) Calculated heat capacity of $CuCrO_2$ and experimental points [41–44,109], figure adapted from our previous work [44].

Using these heat capacity functions and the standard entropy values, the enthalpy of formation of $CuCrO_2$, β and α-$CuCr_2O_4$ and $CuCrO_4$ at 298.15 K were assessed using the reaction temperatures listed in Table 1.

The enthalpy of formation of the β-spinel phase from CuO and Cr_2O_3 ($\Delta_f H°(\alpha\text{-}CuCr_2O_4)$) was estimated at -18819 J/mol, which is significantly smaller than the recent value obtained by Lilova *et al.* [55] (-25190 ± 1830 J/mol). Given the large discrepancy of data reported in the literature (see Table 2), we consider that our value is acceptable. The temperature of the tetragonal transition ($I4_1/amd$) ↔ cubic ($Fd\bar{3}m$) was selected as 583 °C according to [20,21], and the enthalpy for this transition was taken from Lilova *et al.* [55] with a value of - 3030 J/mol.

The variation of log(pO_2) with the reciprocal of the absolute temperature for reactions involving equilibria between $CuCrO_2$ and α-$CuCr_2O_4$ (Eq. 6 and Eq. 7) is plotted in Fig. 10, for our set of thermodynamic functions and available literature data [35,110,111].

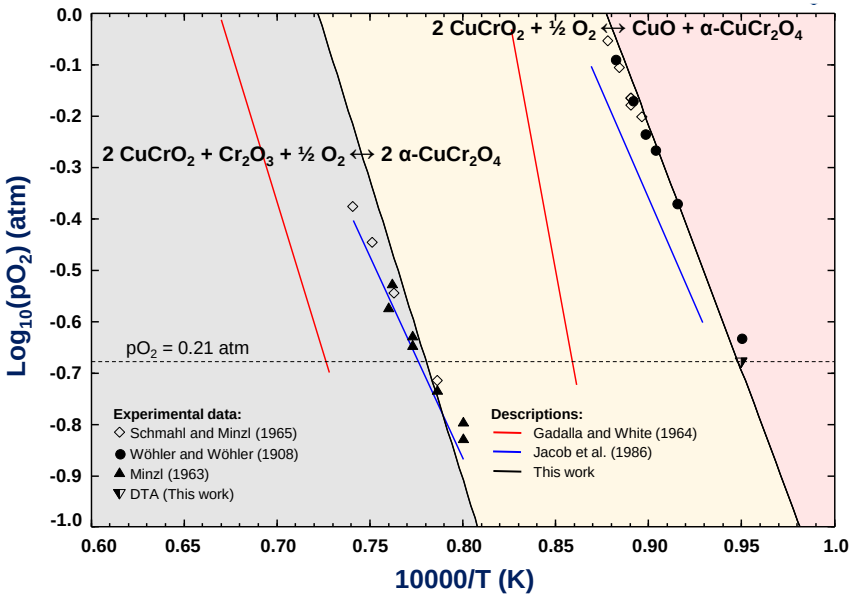

Fig. 10 : Equilibrium oxygen partial pressures in the Cu–Cr–O system for reactions involving equilibria between $CuCrO_2$ and α-$CuCr_2O_4$ (Eq. 7 and Eq. 8). Experimental data from [35,110,111]. Functions from [32,33] and assessment from this work.

Under air atmosphere (i.e. partial pressure of oxygen of 0.21 atm), the calculated temperature for the $CuCrO_2$ formation from CuO and α-$CuCr_2O_4$ (Eq. 6) is 782 °C, in excellent agreement with our measured value of 780 ± 5 °C by TGA (Fig. 4) and also with the overall trend of experimental data. The spinel decomposition temperature (Eq. 7) is calculated as 1010 °C, in good agreement with the values estimated by Jacob *et al.* [33] and Schmahl and Minzl [35] (1012 and 1007 °C, respectively).

As for $CuCrO_4$, our selection of thermodynamic data leads to a stability of this phase under $pO_2 = 1$ atm at low temperature, with a decomposition into β-$CuCr_2O_4$, CuO and $0.5O_2$ at 472 °C, in good agreement with [27,33] (see Table 1). An isothermal section at 427 °C is presented in Fig. 11 to illustrate the resulting computed equilibria at low temperature.

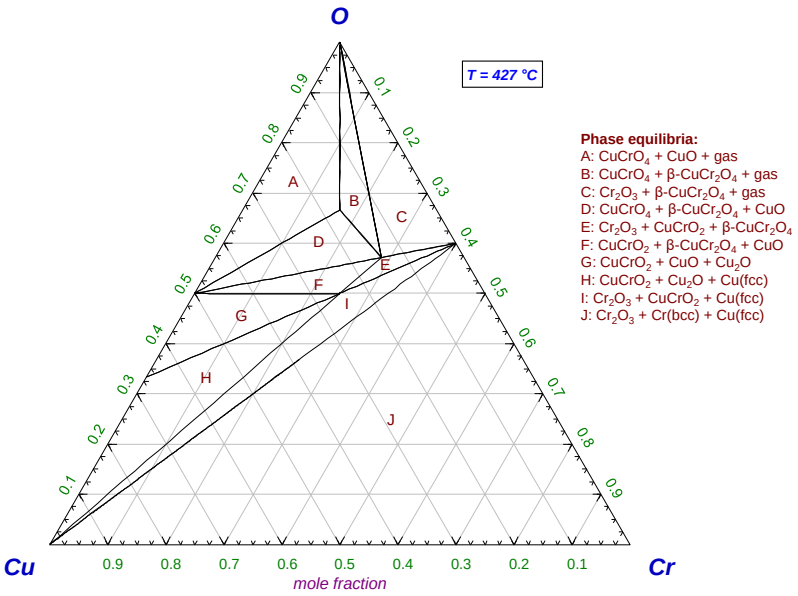

Fig. 11 : Isothermal section of Cr-Cu-O system at 427 °C.

As mentioned in section 2.3, only the solubility of oxygen into the Cr(bcc) has been adjusted to represent the metallic fcc and bcc solutions (Cu,Cr,O), while all the others interaction parameters were accepted from existing works [68,80]. Combined with our assessment of the oxide phases, the resulting computed P_{O_2}-x phase diagram at 1000 °C is presented in Fig. 12. The calculated phase transitions are in good accordance with those proposed by Jacob et al. [33].

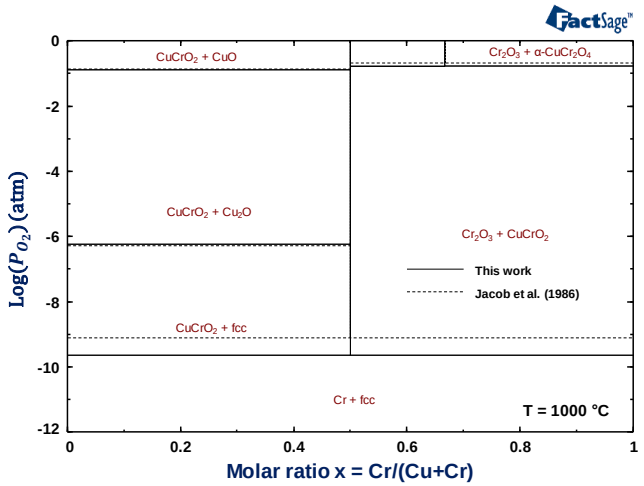

Fig. 12 : Calculated P_{O_2}-x phase diagram of the Cr-Cu-O system at 1000 °C

Assessment of the liquid phase: As discussed in section 2.3, the liquid phase is described by the MQM as (Cu^{1+}, Cu^{2+}, Cr^{1+}, Cr^{2+}, Cr^{3+})(O^{2-}, Va^{1-}). Three ternary interactions (Table 8) were required to fit the unique liquidus data from Hamuyuni and Taskinen [34]. The resulting phase diagram in air is plotted in Fig. 13(a), with a focus around the eutectic (Cr-rich part of the diagram) in Fig. 13(b).

This assessment leads to a decomposition temperature of 1673 °C for the delafossite phase, which is in agreement with the measurement of Gadalla and White [32], who showed that $CuCrO_2$ was stable in air up to at least 1560 °C. No other experimental information is available concerning the stability of the delafossite phase at higher temperature.

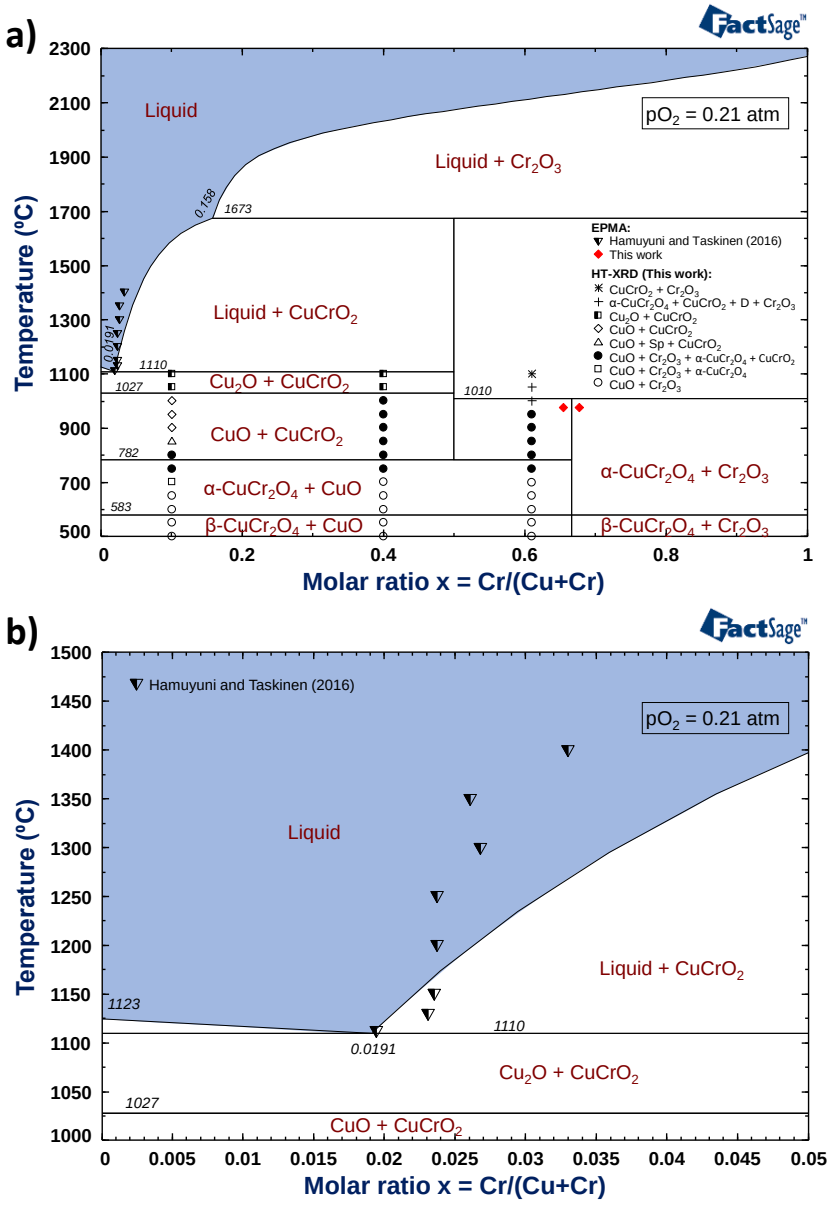

Fig. 13 : Calculated T-x phase diagram of the Cr-Cu-O system in air (a) whole Cu-Cr composition range, (b) focus on the Cr-rich region of the diagram with the only available experimental data.

The calculated coordinates of the eutectic point of the Cu-Cr-O system in air are x = 0.0191, T = 1110 °C, in excellent agreement with the experimental study of Hamuyuni and Taskinen [34] who measured the eutectic at 1112 ± 2 °C and x = 0.0194.

Table 8 : Summary of the optimized model parameters for the solutions of the Cr-Cu-O system (all parameters are in SI units, J, K and mol)

Phase	*Thermodynamic parameters*	*Ref.*
Liquid: $(Cu^{1+},Cu^{2+}, Cr^{1+},Cr^{2+},Cr^{3+})(Va^{1-},O^{2-})$*		
	$^{\circ}G_{Cu^{1+}:Va^{1-}} = G_{Cu(l)}$	*89*
	$^{\circ}G_{Cu^{2+}:Va^{1-}} = G_{Cu(l)} + 150\,000$	**
	$^{\circ}G_{Cr^{1+}:Va^{1-}} = G_{Cr(l)}$	*89*
	$^{\circ}G_{Cr^{2+}:Va^{1-}} = G_{Cr(l)} + 150\,000$	**
	$^{\circ}G_{Cr^{3+}:Va^{1-}} = G_{Cr(l)} + 200\,000$	**
	$^{\circ}G_{Cu^{1+}:O^{2-}} = G_{Cu_2O(l)} + 3\,300$	**
	$^{\circ}G_{Cu^{2+}:O^{2-}} = G_{CuO(l)} + 18\,240$	**
	$^{\circ}G_{Cr^{1+}:O^{2-}} = G_{Cr_2O(l)} + 62\,500$	**
	$^{\circ}G_{Cr^{2+}:O^{2-}} = G_{CrO(l)} + 15\,500$	**
	$^{\circ}G_{Cr^{3+}:O^{2-}} = G_{Cr_2O_3(l)}$	*64*
	$\Delta g_{Cu^{1+},Cr^{1+}/Va^{1-}} = 6\,184.58 + 2.85T + (7\,618.56 - 2.39T)x_{Cr^{1+}Cr^{1+}} + (21756.80 - 12.76T)\,x_{Cu^{1+}Cu^{1+}} - 753.12x^2_{Cu^{1+}Cu^{1+}}$	*67*
	$\Delta g_{Cr^{2+}/Va^{1-},O^{2-}} = -77075 + 25T$	**
	$\Delta g_{Cu^{1+}/Va^{1-},O^{2-}} = 29\,745 - 12.5T + (10\,832 - 8T)\,x_{O^{2-}O^{2-}} + (8\,037 + 6T)\,x_{Va^{1-}Va^{1-}}$	**
	$\Delta g_{Cu^{1+},Cu^{2+}/O^{2-}} = -1\,000 + (13\,540 - 10T)\,x_{Cu^{2+}Cu^{2+}}$	**
	$\Delta g_{Cr^{2+}//Va^{-}O^{2-}} = -77\,075 + 25T$	**
	$\Delta g_{Cu^{1+};Cr^{3+}//O^{2-}} = -20000 + 13.5T$	**
	$\Delta g_{Cu^{2+};Cr^{3+}//O^{2-}} = -17500 + 14T$	**
	$\Delta g_{Cu^{1+};Cr^{3+}//O^{2-}} = (-750 - 0.6T)\,x^2_{Cu^{1+}Cu^{1+}}$	**
	ζ parameters	
	$\zeta_{Cu^{1+}/Va^{1-}} = \zeta_{Cr^{1+}/Va^{1-}} = \zeta_{Cu^{2+}/O^{2-}} = \zeta_{Cr^{2+}/O^{2-}} = 6$	**
	$\zeta_{Cr^{3+}/O^{2-}} = 4.8$	
	$\zeta_{Cu^{2+}/Va^{1-}} = \zeta_{Cr^{2+}/Va^{1-}} = \zeta_{Cr^{1+}/O^{2-}} = \zeta_{Cu^{1+}/O^{2-}} = 4$	
	$\zeta_{Cr^{3+}/Va^{1-}} = 3$	
fcc_A1: $(Cu,Cr,O)_1(Va)_1$		
	$L_{Cu,Cr} = 70672.86 - 15.85T$	*67*
	$L_{Cu,O} = -170498 - 21.00368T$	*68*
bcc_A2: $(Cu,Cr,O)_1(Va)_3$		
	$L_{Cu,Cr} = 70310.40 + 6.04T$	*67*
	$L_{Cr,O} = -152000$	**

* *Second-nearest-neighbor coordination numbers for the quadruplet ABXY (Z_{ABXY}) are provided in Supporting Information*

*** optimized in this work*

Metallic end-members from SGTE

5. Conclusions

In the present work, we have established a thermodynamic description allowing the computation of phase equilibria in the ternary system Cr-Cu-O, based on a careful analysis of available data as well as on a complementary experimental investigation. Several original achievements result from this work:

(i) We performed an experimental measurement (using XRD-HT and TGA-TDA) of the temperature of formation of delafossite in air. The selected value is 780 °C, which confirms previous data from Schmall and Minzl [35] and Jacob et al. [33] (774 and 792 °C, respectively) and rules out the value proposed by Gadalla and White [32] (890 °C).

(ii) We provide experimental evidence (using diffusion couple, microprobe analysis and Rietveld refinement) that neither the spinel nor the delafossite phases exhibit significant cationic non-stoichiometry in the limit of the analysis estimated at x=0.01 (where x is the Cr/(Cu+Cr) molar ratio in the phase).

(iii) We provide, for the first time, an assessment of the thermodynamic functions ($\Delta_f H^{\circ}_{298.15}$, $S^{\circ}_{298.15}$ and $c_p(T)$ polynomial expression) of the $CuCr_2O_4$ spinel up to 1200 K, taking into account the α/β phase transition. The assessment is based on literature data and accounts for equilibria between the various oxide phases for $-1 \leq \log pO_2 \leq 0$.

(iv) We provide an original Calphad model of the Cr-Cu-O system, allowing phase diagram calculation in the whole composition range, including the high-temperature liquid phase described by the modified quasichemical model.

Our recommendation to further improve this thermodynamic description is to carry out high temperature investigations (i.e. higher than 1500 °C) in order to specify the decomposition temperature of the delafossite phase.

ASSOCIATED CONTENT

Supporting Information. Table containing all second-nearest-neighbor coordination numbers for the quadruplet ABXY used in the MQM in the Quadruplet Approximation for the liquid phase (SI_Model_Cr-Cu-O_Z_MQM.docx). Text file containing all model parameters (SI_CuCrO_database.dat). This material is available free of charge via the Internet at http://pubs.acs.org.

AUTHOR INFORMATION

Corresponding Author

* laurent.cassayre@toulouse-inp.fr

Present Addresses

† J.S.P is currently working at the Department of Mechanical Engineering, University of South Carolina, Columbia, South Carolina 29208, USA.

Author Contributions

The manuscript was written through contributions of all authors.

ACKNOWLEDGEMENTS

The authors are grateful for the support of the Région Occitanie (France) for the PhD funding of J.S.P., as well as Toulouse INP for the travel grants of J.S.P. and L.C. at CRCT Montreal. J.S.P., L.C. and A.B. would like to thank Christine Guéneau for her thorough revision of the PhD thesis of J.S.P., which helped to improve the model.
The technical help from S. Le Blond Du Plouy (SEM) and S. Gouy (EPMA) from the Centre de Microcaractérisation Raimond Castaing in Toulouse was greatly appreciated.

REFERENCES

(1) Perrot, P. Chromium – Copper – Oxygen. In *Landolt-Börnstein New Series IV/11E3*; Effenberg, G., Ilyenko, S., Eds.; 110 Materials Science International Services GmbH, 800749, 70507, Stuttgart, Germany, 2010; pp 126–137. https://doi.org/10.1007/978-3-642-00771-2_9.

(2) Milton, C.; Appleman, D. E.; Appleman, M. H.; Chao, E. C. T.; Cuttitta, F.; Dinnin, J. I.; Dwornik, E. J.; Ingram, B. L.; Jr., H. J. R.; Rose, H. J. Merumite; a Complex Assemblage of Chromium Minerals from Guyana. *Prof. Pap.* **1976**, No. 887.

(3) Dannhauser, W.; Vaughan, P. A. The Crystal Structure of Cuprous Chromite. *J. Am. Chem. Soc.* **1955**, *77* (4), 896–897. https://doi.org/10.1021/ja01609a024.

(4) Barnabé, A.; Thimont, Y.; Lalanne, M.; Presmanes, L.; Tailhades, P. P-Type Conducting Transparent Characteristics of Delafossite Mg-Doped CuCrO2 Thin Films Prepared by RF-Sputtering. *J. Mater. Chem. C* **2015**, *3* (23), 6012–6024. https://doi.org/10.1039/C5TC01070E.

(5) Crêpellière, J.; Popa, P. L.; Bahlawane, N.; Leturcq, R.; Werner, F.; Siebentritt, S.; Lenoble, D. Transparent Conductive CuCrO2 Thin Films Deposited by Pulsed Injection Metal Organic Chemical Vapor Deposition: Up-Scalable Process Technology

for an Improved Transparency/Conductivity Trade-Off. *J. Mater. Chem. C* **2016**, *4* (19), 4278–4287. https://doi.org/10.1039/C6TC00383D.

(6) Mahapatra, S.; Shivashankar, S. A. Low-Pressure Metal–Organic Chemical Vapor Deposition of Transparent and p-Type Conducting $CuCrO_2$ Thin Films with High Conductivity. *Chem. Vap. Depos.* **2003**, *9* (5), 238–240. https://doi.org/10.1002/cvde.200304147.

(7) Sinnarasa, I.; Thimont, Y.; Presmanes, L.; Tailhades, P. Thermoelectric and Transport Properties of Delafossite $CuCrO_2$:Mg Thin Films Prepared by RF Magnetron Sputtering. *Nanomaterials* **2017**, *7* (7), 157. https://doi.org/10.3390/nano7070157.

(8) Sinnarasa, I.; Thimont, Y.; Presmanes, L.; Bonningue, C.; Barnabé, A.; Tailhades, P. Influence of Thickness and Microstructure on Thermoelectric Properties of Mg-Doped $CuCrO_2$ Delafossite Thin Films Deposited by RF-Magnetron Sputtering. *Appl. Surf. Sci.* **2018**, *455*, 244–250. https://doi.org/10.1016/j.apsusc.2018.05.104.

(9) Manickam, R.; Biswas, K. Double Doping Induced Power Factor Enhancement in $CuCrO_2$ for High Temperature Thermoelectric Application. *J. Alloys Compd.* **2019**, *775*, 1052–1056. https://doi.org/10.1016/j.jallcom.2018.10.083.

(10) Ketir, W.; Bouguelia, A.; Trari, M. Visible Light Induced NO_2 – Removal Over $CuCrO_2$ Catalyst. *Water. Air. Soil Pollut.* **2009**, *199* (1–4), 115–122. https://doi.org/10.1007/s11270-008-9864-z.

(11) Ma, Y.; Zhou, X.; Ma, Q.; Litke, A.; Liu, P.; Zhang, Y.; Li, C.; Hensen, E. J. M. Photoelectrochemical Properties of $CuCrO_2$: Characterization of Light Absorption and Photocatalytic H_2 Production Performance. *Catal. Letters* **2014**, *144* (9), 1487–1493. https://doi.org/10.1007/s10562-014-1318-1.

(12) Creissen, C. E.; Warnan, J.; Reisner, E. Solar H_2 Generation in Water with a $CuCrO_2$ Photocathode Modified with an Organic Dye and Molecular Ni Catalyst. *Chem. Sci.* **2018**, *9* (6), 1439–1447. https://doi.org/10.1039/C7SC04476C.

(13) Zhao, R.-D.; Zhang, Y.-M.; Liu, Q.-L.; Zhao, Z.-Y. Effects of the Preparation Process on the Photocatalytic Performance of Delafossite $CuCrO_2$. *Inorg. Chem.* **2020**, *59* (22), 16679–16689. https://doi.org/10.1021/acs.inorgchem.0c02678.

(14) Xiong, D.; Xu, Z.; Zeng, X.; Zhang, W.; Chen, W.; Xu, X.; Wang, M.; Cheng, Y.-B. Hydrothermal Synthesis of Ultrasmall $CuCrO_2$ Nanocrystal Alternatives to NiO Nanoparticles in Efficient P-Type Dye-Sensitized Solar Cells. *J. Mater. Chem.* **2012**, *22* (47), 24760. https://doi.org/10.1039/c2jm35101c.

(15) Daniel, U.; Anamaria, D.; Sebarchievicia, I.; Miclau, M. Photovoltaic Performance of Co-Doped $CuCrO_2$ for p-Type Dye-Sensitized Solar Cells Application. *Energy Procedia* **2017**, *112* (October 2016), 497–503. https://doi.org/10.1016/j.egypro.2017.03.1129.

(16) Kaya, I. C.; Akin, S.; Akyildiz, H.; Sonmezoglu, S. Highly Efficient Tandem Photoelectrochemical Solar Cells Using Coumarin6 Dye-Sensitized $CuCrO_2$ Delafossite Oxide as Photocathode. *Sol. Energy* **2018**, *169* (May), 196–205. https://doi.org/10.1016/j.solener.2018.04.057.

(17) Creissen, C. E.; Warnan, J.; Antón-García, D.; Farré, Y.; Odobel, F.; Reisner, E. Inverse Opal CuCrO 2 Photocathodes for H 2 Production Using Organic Dyes and a Molecular Ni Catalyst. *ACS Catal.* **2019**, *9* (10), 9530–9538. https://doi.org/10.1021/acscatal.9b02984.

(18) Maignan, A.; Martin, C.; Frésard, R.; Eyert, V.; Guilmeau, E.; Hébert, S.; Poienar, M.; Pelloquin, D. On the Strong Impact of Doping in the Triangular Antiferromagnet $CuCrO_2$. *Solid State Commun.* **2009**, *149* (23–24), 962–967. https://doi.org/10.1016/j.ssc.2009.02.026.

(19) Bansal, D.; Niedziela, J. L.; May, A. F.; Said, A.; Ehlers, G.; Abernathy, D. L.; Huq, A.; Kirkham, M.; Zhou, H.; Delaire, O. Lattice Dynamics and Thermal Transport in Multiferroic $CuCrO_2$. *Phys. Rev. B* **2017**, *95* (5), 54306. https://doi.org/10.1103/PhysRevB.95.054306.

(20) De, K. S.; Ghose, J.; Murthy, K. S. R. C. Thermal Effects on Cation Distribution of $CuCr_2O_4$. *J. Therm. Anal.* **1981**, *22* (1), 13–16. https://doi.org/10.1007/BF01915690.

(21) Tarantino, S. C.; Giannini, M.; Carpenter, M. A.; Zema, M. Cooperative Jahn–Teller Effect and the Role of Strain in the Tetragonal-to-Cubic Phase Transition in $Mg_xCu_{1-x}Cr_2O_4$. *IUCrJ* **2016**, *3* (5), 354–366. https://doi.org/10.1107/S2052252516012574.

(22) Prasad, R.; Singh, P. Applications and Preparation Methods of Copper Chromite Catalysts: A Review. *Bull. Chem. React. Eng. Catal.* **2011**, *6* (2), 63–114. https://doi.org/10.9767/bcrec.6.2.829.63-113.

(23) Acharyya, S. S.; Ghosh, S.; Bal, R. Catalytic Oxidation of Aniline to Azoxybenzene Over $CuCr_2O_4$ Spinel Nanoparticle Catalyst. *ACS Sustain. Chem. Eng.* **2014**, *2* (4), 584–589. https://doi.org/10.1021/sc5000545.

(24) Liu, P.; Hensen, E. J. M. Highly Efficient and Robust Au/$MgCuCr_2O_4$ Catalyst for Gas-Phase Oxidation of Ethanol to Acetaldehyde. *J. Am. Chem. Soc.* **2013**, *135* (38), 14032–14035. https://doi.org/10.1021/ja406820f.

(25) Mohamed, R. M.; Kadi, M. W. Generation of Hydrogen Gas Using $CuCr_2O_4$ -g-C_3N_4 Nanocomposites under Illumination by Visible Light. *ACS Omega* **2021**, *6* (6), 4485–4494. https://doi.org/10.1021/acsomega.0c06193.

(26) Youn, Y.; Miller, J.; Nwe, K.; Hwang, K.-J.; Choi, C.; Kim, Y.; Jin, S. Effects of Metal Dopings on $CuCr_2O_4$ Pigment for Use in Concentrated Solar Power Solar Selective Coatings. *ACS Appl. Energy Mater.* **2019**, *2* (1), 882–888. https://doi.org/10.1021/acsaem.8b01976.

(27) Jacob, K. T.; Kale, G. M.; Waseda, Y. Gibbs Energy of Formation of $CuCrO_4$ and Phase Relations in the System Cu-Cr-O below 735 K. *Thermochim. Acta* **1992**, *208* (C), 341–348. https://doi.org/10.1016/0040-6031(92)80176-W.

(28) Zienert, T.; Fabrichnaya, O. Thermodynamic Assessment and Experiments in the System MgO–Al_2O_3. *Calphad* **2013**, *40*, 1–9. https://doi.org/10.1016/j.calphad.2012.10.001.

(29) Shishin, D.; Hidayat, T.; Jak, E.; Decterov, S. A. Critical Assessment and Thermodynamic Modeling of the Cu–Fe–O System. *Calphad* **2013**, *41*, 160–179. https://doi.org/10.1016/j.calphad.2013.04.001.

(30) Lindwall, G.; Liu, X. L.; Ross, A.; Fang, H.; Zhou, B.-C.; Liu, Z.-K. Thermodynamic Modeling of the Aluminum–Iron–Oxygen System. *Calphad* **2015**, *51*, 178–192. https://doi.org/10.1016/j.calphad.2015.09.004.

(31) Du, W.-T.; Jung, I.-H. Critical Evaluation and Thermodynamic Modeling of the Fe–V–O (FeO–Fe2O3–VO–V2O3–VO2–V2O5) System. *Calphad* **2019**, *67*, 101682. https://doi.org/10.1016/j.calphad.2019.101682.

(32) Gadalla, A. M. M.; White, J. The System CuO-Cu2O-Cr2O3 and Its Bearing on the Performance of Basis Refractories in Copper-Melting Furnances. *Trans. Brit. Ceram. Soc*. 1964, p 535.

(33) Jacob, K. T.; Kale, G. M.; Iyengar, G. N. K. Oxygen Potentials, Gibbs' Energies and Phase Relations in the Cu-Cr-O System. *J. Mater. Sci.* **1986**, *21* (8), 2753–2758. https://doi.org/10.1007/BF00551483.

(34) Hamuyuni, J.; Taskinen, P. Liquidus Experimental Data for the System Cu-O-Cr2O3 in Air. *Thermochim. Acta* **2016**, *638*, 96–102. https://doi.org/10.1016/j.tca.2016.06.020.

(35) Schmahl, N. G.; Minzl, E. Ermittlung Thermodynamischer Daten von Doppeloxidbildungen Aus Gleichgewichtsmessungen (in German). *Zeitschrift fur Phys. Chemie* **1965**, *47* (5–6), 358–382. https://doi.org/10.1524/zpch.1965.47.5_6.358.

(36) McNally, R. N.; Peters, F. I.; Ribbe, P. H. Laboratory Furnace for Studies in Controlled Atmospheres; Melting Points of MgO in a N2 Atmosphere and of Cr2O3 in N2 and in Air Atmospheres. *J. Am. Ceram. Soc.* **1961**, *44* (10), 491–493. https://doi.org/10.1111/j.1151-2916.1961.tb13711.x.

(37) Schorne-Pinto, J.; Cassayre, L.; Presmanes, L.; Barnabé, A. Insights on the Stability and Cationic Nonstoichiometry of CuFeO2 Delafossite. *Inorg. Chem.* **2019**, *58* (9), 6431–6444. https://doi.org/10.1021/acs.inorgchem.9b00651.

(38) de la Rubia, M. A.; Reinosa, J. J.; Leret, P.; Romero, J. J.; de Frutos, J.; Fernández, J. F. Experimental Determination of the Eutectic Temperature in Air of the CuO–TiO2 Pseudobinary System. *J. Eur. Ceram. Soc.* **2012**, *32* (1), 71–76. https://doi.org/10.1016/j.jeurceramsoc.2011.07.026.

(39) Choudhary, V. R.; Pataskar, S. G. Thermal Analysis of Ammonium Copper Chromate. *J. Therm. Anal.* **1979**, *17* (1), 45–56. https://doi.org/10.1007/BF02156596.

(40) Shabel'skaya, N. P.; Yatsenko, N. D.; Taranushich, V. A.; Khentov, V. Y.; Chernyshev, V. M.; Shabel'skaya, N. P.; Yatsenko, N. D.; Taranushich, V. A.; Khentov, V. Y.; Chernyshev, V. M. Synthesis and Phase Formation in the System Cu–Cr–O. *Glas. Ceram.* **2017**, *74* (1–2), 20–22. https://doi.org/10.1007/s10717-017-9919-y.

(41) Okuda, T.; Beppu, Y.; Fujii, Y.; Onoe, T.; Terada, N.; Miyasaka, S. Specific Heat of Delafossite Oxide CuCr1-x Mgx O2 (0≤x≤0.03). *Phys. Rev. B - Condens. Matter Mater. Phys.* **2008**, *77* (13), 1–5. https://doi.org/10.1103/PhysRevB.77.134423.

(42) Poienar, M.; Damay, F.; Martin, C.; Hardy, V.; Maignan, A.; André, G. Structural and Magnetic Properties of CuCr1-XMgxO2 by Neutron Powder Diffraction. *Phys. Rev. B* **2009**, *79* (1), 14412. https://doi.org/10.1103/PhysRevB.79.014412.

(43) Majee, M. K.; Bhobe, P. A.; Deshpande, U. P.; Nigam, A. K. Local Crystal Structure and Physical Properties Change of p -Type Transparent Conducting Oxide: CuCrO2 upon Ti-Substitution. *J. Appl. Phys.* **2017**, *122* (22), 225111. https://doi.org/10.1063/1.5003965.

(44) Schorne-Pinto, J.; Janghorban, A.; Lomello-Tafin, M.; Pisch, A.; Mikaelian, G.; Benigni, P.; Barnabé, A.; Cassayre, L. Assessment of Thermodynamic Data for CuCrO2 Delafossite from Calorimetric Measurements. *Thermochim. Acta* **2019**, *680*, 178345. https://doi.org/10.1016/j.tca.2019.178345.

(45) Vlach, K. C.; You, Y.-Z.; Austin Chang, Y. A Thermodynamic Study of the Cu-Cr-O System by the EMF Method. *Thermochim. Acta* **1986**, *103* (2), 361–370. https://doi.org/10.1016/0040-6031(86)85173-5.

(46) Ashmore, N. A.; Cann, D. P. Electrical and Structural Characteristics of Non-Stoichiometric Cu-Based Delafossites. *J. Mater. Sci.* **2005**, *40* (15), 3891–3896. https://doi.org/10.1007/s10853-005-0781-x.

(47) Trari, M.; Töpfer, J.; Dordor, P.; Grenier, J. C.; Pouchard, M.; Doumerc, J. P. Preparation and Physical Properties of the Solid Solutions Cu 1+xMn1-XO2 (0≤x≤0.2). *J. Solid State Chem.* **2005**, *178* (9), 2751–2758. https://doi.org/10.1016/j.jssc.2005.06.009.

(48) Ling, D. C.; Chiang, C. W.; Wang, Y. F.; Lee, Y. J.; Yeh, P. H. Effect of Cr Deficiency on Physical Properties of Triangular-Lattice Antiferromagnets CuCr1-XO2 (0≦x≦0.10). *J. Appl. Phys.* **2011**, *109* (7), 07D908. https://doi.org/10.1063/1.3544498.

(49) Singh, S. B.; Yang, L. T.; Wang, Y. F.; Shao, Y. C.; Chiang, C. W.; Chiou, J. W.; Lin, K. T.; Chen, S. C.; Wang, B. Y.; Chuang, C. H.; Ling, D. C.; Pong, W. F.; Tsai, M.-H.; Tsai, H. M.; Pao, C. W.; Shiu, H. W.; Chen, C. H.; Lin, H.-J.; Lee, J. F.; Yamane, H.; Kosugi, N. Correlation between P-Type Conductivity and Electronic Structure of Cr-Deficient CuCr1-XO2 (X=0-0.1). *Phys. Rev. B* **2012**, *86* (24), 241103. https://doi.org/10.1103/PhysRevB.86.241103.

(50) Tretjakow, J. D.; Schmalzried, H. Zur Thermodynamik von Spinellphasen. (Chromite, Ferrite, Aluminate). *Berichte der Bunsengesellschaft für Phys. Chemie* **1965**, *69* (5), 396–402. https://doi.org/10.1002/bbpc.19650690506.

(51) Yé, Z.-G. G.; Crottaz, O.; Vaudano, F.; Kubel, F.; Tissot, P.; Schmid, H. Single Crystal Growth, Structure Refinement, Ferroelastic Domains and Phase Transitions of the Hausmannite CuCr2O4. *Ferroelectrics* **1994**, *162* (1), 103–118. https://doi.org/10.1080/00150199408245096.

(52) Holla, H. Double Oxides: Thermodynamic Properties and Phase Equilibria, Ohio State University, 1995.

(53) Jain, A.; Hautier, G.; Ong, S. P.; Moore, C. J.; Fischer, C. C.; Persson, K. A.; Ceder, G. Formation Enthalpies by Mixing GGA and GGA + U Calculations. *Phys. Rev. B - Condens. Matter Mater. Phys.* **2011**, *84* (4), 1–10. https://doi.org/10.1103/PhysRevB.84.045115.

(54) Müller, F.; Kleppa, O. J. Thermodynamics of Formation of Chromite Spinels. *J. Inorg. Nucl. Chem.* **1973**, *35* (8), 2673–2678. https://doi.org/10.1016/0022-1902(73)80497-X.

(55) Lilova, K.; Sharma, G.; Hayun, S.; Shoemaker, D. P.; Navrotsky, A. Thermodynamics of ZnxMn3–xO4 and Mg1–zCuzCr2O4 Spinel Solid Solutions. *J. Mater. Res.* **2019**, *34* (19), 3305–3311. https://doi.org/10.1557/jmr.2019.196.

(56) Inaba, H.; Yagi, H.; Naito, K. Heat Capacity Anomalies Due to the Cooperative Jahn-Teller Effect in Cu1–xNixCr2O4. *J. Solid State Chem.* **1986**, *64* (1), 67–75. https://doi.org/10.1016/0022-4596(86)90122-2.

(57) Suchomel, M. R.; Shoemaker, D. P.; Ribaud, L.; Kemei, M. C.; Seshadri, R. Spin-Induced Symmetry Breaking in Orbitally Ordered NiCr2O4 and CuCr2O4. *Phys. Rev. B* **2012**, *86* (5), 54406. https://doi.org/10.1103/PhysRevB.86.054406.

(58) Tomiyasu, K.; Lee, S.; Ishibashi, H.; Takahashi, Y.; Kawamata, T.; Koike, Y.; Nojima, T.; Torii, S.; Kamiyama, T. Emergence of Spin-Orbit Order in the Spinel CuCr2O4. *Strongly Correl. Electrons* **2018**, 1–10.

(59) Law, J. M.; Reuvekamp, P.; Glaum, R.; Lee, C.; Kang, J.; Whangbo, M.-H.; Kremer, R. K. Quasi-One-Dimensional Antiferromagnetism and Multiferroicity in CuCrO4. *Phys. Rev. B* **2011**, *84* (1), 14426. https://doi.org/10.1103/PhysRevB.84.014426.

(60) Pelton, A. *Phase Diagrams and Thermodynamic Modeling of Solutions*; Elsevier, 2018.

(61) Lalanne, M.; Barnabé, A.; Mathieu, F.; Tailhades, P. Synthesis and Thermostructural Studies of a CuFe1-XCr XO2 Delafossite Solid Solution with 0 ≤ × ≤ 1. *Inorg. Chem.* **2009**, *48* (13), 6065–6071. https://doi.org/10.1021/ic900437x.

(62) Rietveld, H. M. A Profile Refinement Method for Nuclear and Magnetic Structures. *J. Appl. Crystallogr.* **1969**, *2* (2), 65–71. https://doi.org/10.1107/S0021889869006558.

(63) Rodríguez-Carvajal, J. Recent Advances in Magnetic Structure Determination by Neutron Powder Diffraction. *Phys. B Condens. Matter* **1993**, *192* (1–2), 55–69. https://doi.org/10.1016/0921-4526(93)90108-I.

(64) Bale, C. W.; Bélisle, E.; Chartrand, P.; Decterov, S. A.; Eriksson, G.; Gheribi, A. E.; Hack, K.; Jung, I.-H.; Kang, Y.-B.; Melançon, J.; Pelton, A. D.; Petersen, S.; Robelin, C.; Sangster, J.; Spencer, P.; Van Ende, M.-A. FactSage Thermochemical Software and Databases, 2010–2016. *Calphad* **2016**, *54*, 35–53. https://doi.org/10.1016/j.calphad.2016.05.002.

(65) Maier, C. G.; Kelley, K. K. An Equation for the Representation of High-Temperature Heat Content Data. *J. Am. Chem. Soc.* **1932**, *54* (8), 3243–3246. https://doi.org/10.1021/ja01347a029.

(66) Redlich, O.; Kister, A. T. Algebraic Representation of Thermodynamic Properties and the Classification of Solutions. *Ind. Eng. Chem.* **1948**, *40* (2), 345–348. https://doi.org/10.1021/ie50458a036.

(67) Cui, S.; Jung, I.-H. Thermodynamic Modeling of the Cu-Fe-Cr and Cu-Fe-Mn Systems. *Calphad* **2017**, *56*, 241–259. https://doi.org/10.1016/j.calphad.2017.01.004.

(68) Shishin, D.; Decterov, S. A. Critical Assessment and Thermodynamic Modeling of the Cu-O and Cu-O-S Systems. *Calphad Comput. Coupling Phase Diagrams Thermochem.* **2012**, *38*, 59–70. https://doi.org/10.1016/j.calphad.2012.04.002.

(69) Saunders, N. Thermodynamic Characterization of Cu–Cr System. *Mater. Sci. Technol.* **1987**, *3* (8), 671–673. https://doi.org/10.1179/mst.1987.3.8.671.

(70) Hämäläinen, M.; Jääskeläinen, K.; Luoma, R.; Nuotio, M.; Taskinen, P.; Teppo, O. A Thermodynamic Analysis of the Binary Alloy Systems Cu-Cr, Cu-Nb and Cu-V. *Calphad* **1990**, *14* (2), 125–137. https://doi.org/10.1016/0364-5916(90)90014-Q.

(71) Zeng, K.; Hämäläinen, M. Thermodynamic Analysis of Stable and Metastable Equilibria in the Cu-Cr System. *Calphad* **1995**, *19* (1), 93–104. https://doi.org/10.1016/0364-5916(95)00010-C.

(72) Turchanin, M. A. Phase Equilibria and Thermodynamics of Binary Copper Systems with 3d-Metals. III. Copper-Chromium System. *Powder Metall. Met. Ceram.* **2006**, *45* (9–10), 457–467. https://doi.org/10.1007/s11106-006-0106-x.

(73) Hallstedt, B.; Risold, D.; Gauckler, L. J. Thermodynamic Assessment of the Copper-Oxygen System. *J. Phase Equilibria* **1994**, *15* (5), 483–499. https://doi.org/10.1007/BF02649399.

(74) Hallstedt, B.; Gauckler, L. J. Revision of the Thermodynamic Descriptions of the Cu–O, Ag–O, Ag–Cu–O, Bi–Sr–O, Bi–Ca–O, Bi–Cu–O, Sr–Cu–O, Ca–Cu–O and Sr–Ca–Cu–O Systems. *Calphad* **2003**, *27* (2), 177–191. https://doi.org/10.1016/S0364-5916(03)00050-6.

(75) Clavaguera-Mora, M. T.; Touron, J. L.; Rodríguez-Viejo, J.; Clavaguera, N. Thermodynamic Description of the Cu-O System. *J. Alloys Compd.* **2004**, *377* (1–2), 8–16. https://doi.org/10.1016/j.jallcom.2004.01.031.

(76) Schramm, L.; Behr, G.; Löser, W.; Wetzig, K. Thermodynamic Reassessment of the Cu-O Phase Diagram. *J. Phase Equilibria Diffus.* **2005**, *26* (6), 605–612. https://doi.org/10.1007/s11669-005-0005-8.

(77) Taylor, J. R.; Dinsdale, A. T. Thermodynamic Assessment of the Ni-O, Cr-O and Cr-Ni-O Systems Using the Ionic Liquid and Compound Energy Models. *Zeitschrift fuer Met.* **1990**, *81* (5), 354–366.

(78) Kowalski, M.; Spencer, P. J. Thermodynamic Reevaluation of the Cr-O, Fe-O and Ni-O Systems: Remodelling of the Liquid, BCC and FCC Phases. *Calphad* **1995**, *19* (3), 229–243. https://doi.org/10.1016/0364-5916(95)00024-9.

(79) Luoma, R. A Thermodynamic Analysis of the System Fe-Cr-Ni-C-O, Acta Polytechnica Scandinavica, 2002.

(80) Povoden, E.; Nicholas Grundy, A.; Gauckler, L. J. Thermodynamic Reassessment of the Cr–O System in the Framework of Solid Oxide Fuel Cell (SOFC) Research. *J. Phase Equilibria Diffus.* **2006**, *27* (4), 353–362. https://doi.org/10.1007/s11669-006-0007-1.

(81) Kjellqvist, L.; Selleby, M.; Sundman, B. Thermodynamic Modelling of the Cr–Fe–Ni–O System. *Calphad* **2008**, *32* (3), 577–592. https://doi.org/10.1016/j.calphad.2008.04.005.

(82) Pelton, A. D.; Degterov, S. A.; Eriksson, G.; Robelin, C.; Dessureault, Y. The Modified Quasichemical Model I—Binary Solutions. *Metall. Mater. Trans. B* **2000**, *31* (4), 651–659. https://doi.org/10.1007/s11663-000-0103-2.

(83) Pelton, A. D.; Chartrand, P. The Modified Quasi-Chemical Model: Part II. Multicomponent Solutions. *Metall. Mater. Trans. A* **2001**, *32* (6), 1355–1360. https://doi.org/10.1007/s11661-001-0226-3.

(84) Lambotte, G.; Chartrand, P. Thermodynamic Optimization of the (Na2O + SiO2 + NaF + SiF4) Reciprocal System Using the Modified Quasichemical Model in the Quadruplet Approximation. *J. Chem. Thermodyn.* **2011**, *43* (11), 1678–1699. https://doi.org/10.1016/j.jct.2011.05.038.

(85) Sato, K.; Kamishima, K.; Kakizaki, K.; Hiratsuka, N. Magnetoresistance in Cu Ferrite System (in Japanese). *J. Japan Soc. Powder Powder Metall.* **2004**, *51* (9), 708–712. https://doi.org/10.2497/jjspm.51.708.

(86) Sahu, S. K.; Navrotsky, A. Thermodynamics of Copper-manganese and Copper-iron Spinel Solid Solutions. *J. Am. Ceram. Soc.* **2017**, *100* (8), 3684–3692. https://doi.org/10.1111/jace.14813.
(87) Doumerc, J.-P.; Ammar, A.; Wichainchai, A.; Pouchard, M.; Hagenmuller, P. Sur Quelques Nouveaux Composes de Structure de Type Delafossite (in French). *J. Phys. Chem. Solids* **1987**, *48* (1), 37–43. https://doi.org/10.1016/0022-3697(87)90140-5.
(88) Lunca Popa, P.; Crêpellière, J.; Nukala, P.; Leturcq, R.; Lenoble, D. Invisible Electronics: Metastable Cu-Vacancies Chain Defects for Highly Conductive p-Type Transparent Oxide. *Appl. Mater. Today* **2017**, *9*, 184–191. https://doi.org/10.1016/j.apmt.2017.07.004.
(89) Dinsdale, A. T. SGTE Data for Pure Elements. *Calphad* **1991**, *15* (4), 317–425. https://doi.org/10.1016/0364-5916(91)90030-N.
(90) Hallstedt, B.; Risold, D.; Gauckler, L. J. Thermodynamic Assessment of the Copper-Oxygen System. *J. Phase Equilibria* **1994**, *15* (5), 483–499. https://doi.org/10.1007/BF02649399.
(91) Heyn, E. Kupfer Und Sauerstoff (in German). *Zeitschrift für Anorg. Chemie* **1904**, *39* (1), 1–23. https://doi.org/10.1002/zaac.19040390102.
(92) Roberts, H. S.; Smyth, F. H. The System Copper: Cupric Oxide: Oxygen. *J. Am. Chem. Soc.* **1921**, *43* (5), 1061–1079. https://doi.org/10.1021/ja01438a009.
(93) Osterwald, J. EMK-Messungen an Flüssigem Kupfer Im Gleichgewicht Mit Festem Oder Flüssigem Kupfer(I)-Oxid (in German). *Zeitschrift für Phys. Chemie* **1966**, *49* (3_5), 138–146. https://doi.org/10.1524/zpch.1966.49.3_5.138.
(94) Rickert, H.; Wagner, H.; Steiner, R. Elektrochemische Messung Der Sauerstoff-Aktivität Und -Diffusion in Metallen Mit Zirkondioxid Als Festelektrolyt (in German). *Chemie Ing. Tech. - CIT* **1966**, *38* (6), 618–622. https://doi.org/10.1002/cite.330380605.
(95) Kuxmann, U.; Kurre, K. Die Mischungslucke Im System Kupfer-Sauerstoff Und Ihre Beeinflussung Durch Die Oxide CaO, SiO2, Al2O3, MgO, Al2O3 Und ZrO2 (in German). *Erzmetall* **1968**, *21* (5), 199–209.
(96) Gerlach, G.; Osterwald, G.; Stichel, W. Coulometrische Bestimmung Der Mischungslücke Zwischen Flüssigem Kupfer Und Kupfer(I)-Oxid (in German). *Z. Met.* **1968**, *59*, 576–579.
(97) Sadat-Darbandi, S. Determination of Equilibrium and Transport Properties of the Liquid Phases of the System Copper-Oxygen (in German), TU Berlin, 1977.
(98) Kemori, N.; Katayama, I.; Kozuka, Z. Thermodynamic Study of Oxygen in Liquid Copper. *Trans. Japan Inst. Met.* **1980**, *21* (5), 275–284. https://doi.org/10.2320/matertrans1960.21.275.
(99) Kayahara, Y.; Ono, K.; Oishi, T.; Moriyama, J. Thermodynamic Study of the Liquid Cu-O System. *Trans. Japan Inst. Met.* **1981**, *22* (7), 493–500. https://doi.org/10.2320/matertrans1960.22.493.
(100) Taskinen, P. The Standard Gibbs Energy of Formation of Cu2O(s) at 1066-1220 C. *Scand. J. Met.* **1981**, *10* (4), 189–191.
(101) Kosenko, A. V.; Emel'chenko, G. A. Equilibrium Phase Relationships in the System Cu-O under High Oxygen Pressure. *J. Phase Equilibria* **2001**, *22* (1), 12–19. https://doi.org/10.1007/s11669-001-0050-x.
(102) Osterwald, J. Ueber Das Zustandsdiagramm Des Systems Kupfer-Sauerstoff Im Temperaturbereich Fluessiger Phasen (in German). *Zeitschrift fuer Met.* **1968**, *59* (7), 573–576.
(103) Toker, N. Y.; Darken, L. S.; Muan, A. Equilibrium Phase Relations and Thermodynamics of the Cr-o System in the Temperature Range of 1500 °C to 1825 °C. *Metall. Trans. B* **1991**, *22* (2), 225–232. https://doi.org/10.1007/BF02652487.
(104) Ol'shanskii, Y. I.; Shlepov, V. K. Sistema Cr–Cr2O3 (in Russian). *Dokl. Akad. Nauk SSSR* **1953**, *91* (3), 561–564.
(105) Ramsey, J. N.; Caplan, D.; Burr, A. A. Thermodynamics of the Oxidation of Chromium. *J. Electrochem. Soc.* **1956**, *103* (2), 135. https://doi.org/10.1149/1.2430244.
(106) Davies, H.; Smeltzer, W. W. Oxygen and Metal Activities of the Chromium-Nickel-Oxygen System Between 900° and 1100°C. *J. Electrochem. Soc.* **1974**, *121* (4), 543. https://doi.org/10.1149/1.2401857.
(107) Neumann, C.; Saalfeld, H. III. Investigations of the Specific Heat of Solid Bodies. *Philos. Trans. R. Soc. London* **1865**, *155* (3–4), 71–202. https://doi.org/10.1098/rstl.1865.0003.
(108) Kubaschewski, O.; Alcock, C. B.; J, P. S. 5. Thermochemical Data. In *Materials thermochemistry*; Pergamon Press: Oxford ; New York, 1993; p 363.
(109) Kimura, K.; Nakamura, H.; Ohgushi, K.; Kimura, T. Magnetoelectric Control of Spin-Chiral Ferroelectric Domains in a Triangular Lattice Antiferromagnet. *Phys. Rev. B* **2008**, *78* (14), 140401. https://doi.org/10.1103/PhysRevB.78.140401.
(110) Wöhler, L.; Wöhler, P. Über Die Dissociation von Chromoxyden Und Kupfer-Chromoxyden (in German). *Zeitschrift für Phys. Chemie* **1908**, *62U* (1). https://doi.org/10.1515/zpch-1908-6226.
(111) Minzl, E. Doctoral Thesis, Universität Saarbrücken, 1993.

For Table of Contents Only

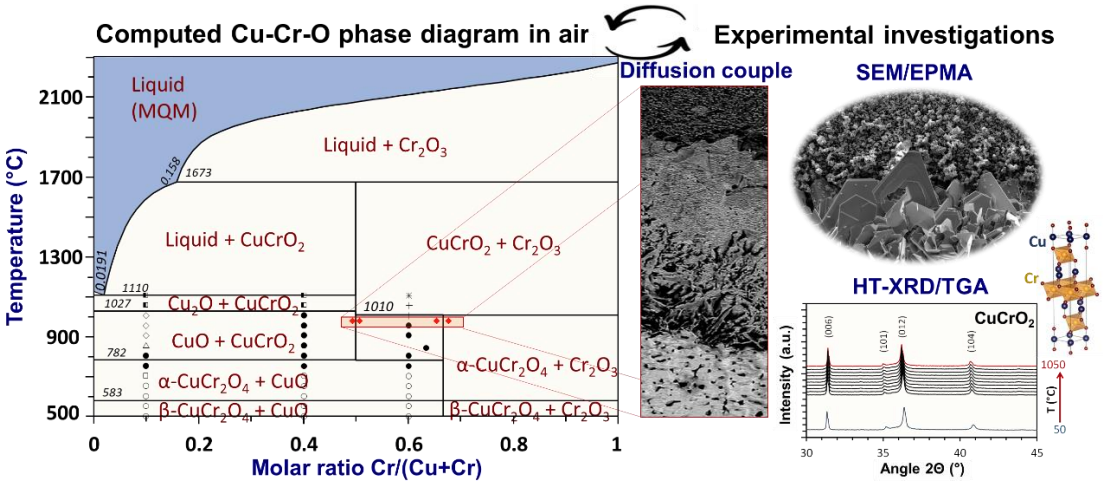
Computed Cu-Cr-O phase diagram in air
Experimental investigations
Diffusion couple
SEM/EPMA
HT-XRD/TGA
Liquid (MQM)
Liquid + Cr_2O_3
Liquid + $CuCrO_2$
$CuCrO_2$ + Cr_2O_3
Cu_2O + $CuCrO_2$
CuO + $CuCrO_2$
α-$CuCr_2O_4$ + CuO
β-$CuCr_2O_4$ + CuO
α-$CuCr_2O_4$ + Cr_2O_3
β-$CuCr_2O_4$ + Cr_2O_3
Temperature (°C)
Molar ratio Cr/(Cu+Cr)
Intensity (a.u.)
Angle 2Θ (°)
$CuCrO_2$
Cu
Cr
T (°C)